

INVESTIGATION OF PARAMETERS AFFECTING MORPHOLOGY OF
MICROFILTRATION AND ULTRAFILTRATION MEMBRANES FABRICATED
VIA PHASE SEPARATION MICROFABRICATION

A THESIS SUBMITTED TO
THE GRADUATE SCHOOL OF NATURAL AND APPLIED SCIENCES
OF
MIDDLE EAST TECHNICAL UNIVERSITY

BY

CANKUT KAAAN BOLAT

IN PARTIAL FULFILLMENT OF THE REQUIREMENTS
FOR
THE DEGREE OF MASTER OF SCIENCE
IN
CHEMICAL ENGINEERING

AUGUST 2017

Approval of the thesis:

**INVESTIGATION OF PARAMETERS AFFECTING MORPHOLOGY OF
MICROFILTRATION AND ULTRAFILTRATION MEMBRANES
FABRICATED VIA PHASE SEPARATION MICROFABRICATION**

Submitted by **CANKUT KAAN BOLAT** in partial fulfillment of the requirements for the degree of **Master of Science in Chemical Engineering Department, Middle East Technical University** by,

Prof. Dr. Gülbin Dural Ünver _____

Dean, **Graduate School of Natural and Applied Sciences**

Prof. Dr. Halil Kalıpçılar _____

Head of Department, **Chemical Engineering**

Assoc. Prof. Dr. Pınar Zeynep Çulfaz Emecen _____

Supervisor, **Chemical Engineering Dept., METU**

Asst. Prof. Dr. Erhan Bat _____

Co-Supervisor, **Chemical Engineering Dept., METU**

Examining Committee Members:

Prof. Dr. Levent Yılmaz _____

Chemical Engineering Dept., METU

Assoc. Prof. Dr. Pınar Zeynep Çulfaz Emecen _____

Chemical Engineering Dept., METU

Asst. Prof. Dr. Erhan Bat _____

Chemical Engineering Dept., METU

Prof. Dr. Halil Kalıpçılar _____

Chemical Engineering Dept., METU

Asst. Prof. Dr. Enver Güler _____

Faculty of Engineering, Chemical Engineering
and Applied Chemistry, Atılım University

Date: 21.08.2017

I hereby declare that all the information in this document has been obtained and presented in accordance with academic rules and ethical conduct. I also declare that, as required by these rules and conduct, I have fully cited and referenced all material and results that are not original to this work.

Name, Last Name: Cankut Kaan Bolat

Signature:

ABSTRACT

INVESTIGATION OF PARAMETERS AFFECTING MORPHOLOGY OF MICROFILTRATION AND ULTRAFILTRATION MEMBRANES FABRICATED VIA PHASE SEPARATION MICROFABRICATION

Bolat, Cankut Kaan

M.Sc., Department of Chemical Engineering

Supervisor: Assoc. Prof. Dr. Pınar Zeynep Çulfaz Emecen

Co-Supervisor: Asst. Prof. Dr. Erhan Bat

August 2017, 76 pages

This study examines the factors affecting the morphology of polyethersulfone membranes produced via phase separation microfabrication technique. Flat and corrugated membranes were prepared using a combination of vapor induced and liquid induced phase separation, and characterized using scanning electron microscopy, pure water permeance tests and Baker's yeast (*Saccharomyces Cerevisiae*) fouling tests.

An inverse asymmetric morphology was tried to be achieved for corrugated membranes, in order to increase the effectiveness of filtration for a polymer solution containing 10% polyethersulfone, 60% polyethylene glycol (PEG-400), 25% N-methyl-2-pyrrolidone (NMP) and 5% pure water by weight. Membrane morphologies were tried to be tuned by altering humid air flow rate, humid air exposure time and relative humidity during vapor induced phase separation. Results showed that the closest structure to desired inverse asymmetric membrane was the membrane

exposed to humid air for 4 minutes at 80% relative humidity with the flow rate of 0.9 L/min, which was chosen with its flat counterpart for further investigation.

Chosen membranes were also exposed to polydopamine coating for pore size reduction and increasing the surface hydrophilicity. Coated and uncoated membranes were compared for their pure water permeance and fouling during yeast filtration.

Polydopamine coating decreased the pure water permeance on both type of membranes as expected, however all the membranes performed no rejection to BSA solutions. Moreover, it was observed that polydopamine coated membranes have shown worse fouling performances when compared to their uncoated counterparts. Corrugated membranes had higher pure water permeances and better fouling behavior compared to their flat counterparts.

Keywords: Membrane, microfiltration, fouling, corrugated membrane, polydopamine.

ÖZ

FAZ AYIRMA MİKRO ÜRETİM TEKNİĞİ İLE ÜRETİLEN MİKROFİLTRASYON VE ULTRAFİLTRASYON MEMBRAN MORFOLOJİLERİNİ ETKİLEYEN PARAMETRELERİN ARAŞTIRILMASI

Bolat, Cankut Kaan

Yüksek Lisans, Kimya Mühendisliği Bölümü

Tez Yöneticisi: Assoc. Prof. Dr. Pınar Zeynep Çulfaz Emecen

Ortak Tez Yöneticisi: Asst. Prof. Dr. Erhan Bat

Ağustos 2014, 76 sayfa

Bu çalışma faz ayırma mikro üretim tekniği ile üretilen polietersülfon membranların morfolojilerini etkileyen faktörleri incelemektedir. Buhar ile ve sıvı ile faz ayırma yöntemlerinin birleşimi kullanılarak düz ve oluklu membranlar üretilmiş, bu membranlar taramalı electron mikroskobu, saf su geçirgenliği ve ekme mayası (*Saccharomyces Cerevisiae*) kirlenme testleriyle karakterize edilmiştir.

Kütlece %10 polietersülfon, %60 polietilen glikol (PEG-400), %25 N-metil-2-pirolidon (NMP) ve %5 saf su içeren polimer çözeltileriyle dökülen oluklu membranlarda filtrasyon verimini arttırmak adına ters asimetric yapıya ulaşmak hedeflenmiştir. Buharla faz değiştirme işlemi esnasında nemli hava akış hızı, nemli havaya maruz kalma süresi ve bağıl nem değiştirilerek membran morfolojisi ayarlanmaya çalışılmıştır. Sonuçlar istenen ters asimetric yapıya en yakın yapının 0.9 L/dk akış hızında yüzde seksen bağıl neme 4 dakika maruz kalan membranlarda olduğunu göstermektedir, bu yüzden bu membranın oluklu ve düz halleri araştırmanın ileriki aşamaları için uygun görülmüştür.

Seçilen membranlar ayrıca gözenek boyutlarını küçültebilmek ve yüzey hidrofiliğini arttırmak adına polidopamin ile kaplanmıştır. Kaplanmış ve kaplanmamış membranlar saf su geçirgenliği ve maya filtrasyonu sırasında kirlenme testlerine tabi tutulmuşlardır.

Polidopamin kaplama beklendiği gibi hem düz hem oluklu membranların saf su geçirgenliğini azaltmıştır, fakat tüm membranlar hala BSA geçirmeye devam etmiştir. Buna ek olarak, beklenenin aksine polidopamin kaplanan membranların kaplanmamış olanlara göre daha çok kirlendiği gözlenmiştir. Oluklu membranların düz muadillerine göre daha yüksek saf su geçirgenliği gösterdiği ve filtrasyon sırasında daha az kirlendiği gözlemlenmiştir.

Anahtar Kelimeler: Membran, mikrofiltrasyon, kirlenme, oluklu membran, polidopamin.

To My Beloved Family.

ACKNOWLEDGEMENTS

I would like to thank to my supervisor Assoc. Prof. Pınar Zeynep Çulfaz Emecen for all the support, guidance and help she has given me throughout my study. I know I have not been the easiest of the students, and I know I would not be able to progress without her endless patience and vision. It has been an honor to have worked with and learned from her. That being said, I would also like to thank to my co-supervisor Erhan Bat for being an impressive mentor, for convincing me to start my graduate studies in chemical engineering and for guiding me whenever I needed since we have met.

Of course a huge shout out must go to the membrane girls; to Faqih for teaching me the true meaning of humble, to Elif who basically taught the way around our laboratory and personally the way around my own life, to Hazal for all the dessert and health tips, to Kübra for her endless joy and positive mood at the darkest of times, to Begüm for just listening to me whenever I complain, and to Zeynep for showing me one of the smartest senses of humor I have ever seen. It is my pleasure to have known and worked with them, and I wish each of them the best from my heart.

I owe more than words could express to my dearest parents, who always accepted me the way I am and supported my stupidest decisions. Thank you for always making me feel like the luckiest person on earth.

Finally, I have to thank to each one of my beloved Unicorns from the bottom of my heart. Without their support, endless love and trust, I could not achieve anything I achieved for the past three years. Ahmet Can and Emre for being there for me at the most stressed times when I was writing my thesis, Can and Kamil for being my musketeers, Sila for just loving me despite me, and Faykurt for just being himself.

TABLE OF CONTENTS

| | |
|--|------|
| ABSTRACT..... | v |
| ÖZ | vii |
| ACKNOWLEDGEMENTS | x |
| TABLE OF CONTENTS..... | xi |
| LIST OF TABLES | xiii |
| LIST OF FIGURES | xiv |
| CHAPTERS | |
| 1. INTRODUCTION | 1 |
| 1.1. Membranes and Filtration | 1 |
| 1.2. Phase Separation Micro-Molding | 3 |
| 1.3. Factors Affecting Membrane Performances | 6 |
| 1.4. Preventing the Effects of Concentration Polarization and Fouling..... | 10 |
| 1.5. Patterned Membranes..... | 12 |
| 1.6. Polydopamine Coating | 15 |
| 1.7. Aim of the Study | 19 |
| 2. EXPERIMENTAL METHODS..... | 21 |
| 2.1. Materials..... | 21 |
| 2.2. Membrane Casting | 21 |
| 2.2.1. Solution Preparation..... | 21 |
| 2.2.2. Flat Membranes..... | 22 |
| 2.2.3. Corrugated Membranes | 23 |
| 2.3. Polydopamine Coating | 24 |

| | |
|---|----|
| 2.4. Performance and Morphology Observations..... | 26 |
| 2.4.1. Morphology and Characterization..... | 26 |
| 2.4.2. Pure Water Permeance Tests..... | 27 |
| 2.4.3. BSA Rejection Tests..... | 30 |
| 2.4.4. Yeast Fouling Tests..... | 30 |
| 3. RESULTS AND DISCUSSION..... | 33 |
| 3.1 Membrane Morphologies..... | 33 |
| 3.1.1. Effect of Humid Air Flow Rate..... | 36 |
| 3.1.2. Effect of Humid Air Exposure Time..... | 39 |
| 3.1.3. Effect of Relative Humidity..... | 43 |
| 3.2. Performance Tests..... | 52 |
| 3.2.1. Pure Water Permeances..... | 52 |
| 3.2.2. Fouling Performances..... | 57 |
| 4. CONCLUSIONS..... | 61 |
| REFERENCES..... | 63 |
| APPENDICES..... | 69 |
| A. P/PWP VALUES FOR THE MEMBRANES..... | 69 |
| B. CALCULATION OF REYNOLDS NUMBERS AND PWP..... | 71 |
| C. BSA REJECTION CALCULATIONS..... | 73 |
| D. FOULING RESISTANCE CALCULATIONS..... | 75 |

LIST OF TABLES

TABLES

| | |
|--|----|
| Table 3.1 Pore Sizes of Membranes Exposed to Different Humid Air Flow Rates..... | 38 |
| Table 3.2 Dimensions of Corrugated Membranes Exposed to Humid Air at 80% Relative Humidity 0.9 L/min and 1.6 L/min for 5 minutes | 39 |
| Table 3.3 Pore Sizes of Membranes Having Different Exposure Times | 42 |
| Table 3.4 Dimensions of Corrugated Membranes Exposed to Humid Air at 80% Relative Humidity 0.9 L/min for 5, 4 and 3 Minutes..... | 43 |
| Table 3.5 Dimensions of Corrugated Membranes Exposed to Humid Air at 50% Relative Humidity | 45 |
| Table 3.6 Cross Sectional SEM Images of Flat Membranes | 47 |
| Table 3.7 Thickness Values of Flat Membranes | 49 |
| Table 3.8 Flat Membrane Pore Sizes | 50 |
| Table 3.9 Elemental Weight Percentages taken from EDX Results of Uncoated and Polydopamine Coated Membranes | 55 |

LIST OF FIGURES

FIGURES

| | |
|---|----|
| Figure 1.1 A Simple Drawing of a Membrane Filtration..... | 2 |
| Figure 1.2 Simple Schematics of Symmetric and Asymmetric Membranes..... | 3 |
| Figure 1.3 Ternary Phase Diagram Sample for a Non Solvent Induced Phase Separation Process..... | 4 |
| Figure 1.4 A Typical Phase Separation Micro Molding Process | 6 |
| Figure 1.5 Simple Representation of Concentration Polarization..... | 7 |
| Figure 1.6 Representation of Flow Resistances During Filtration | 9 |
| Figure 1.7 Representation of Corrugations on the Flow | 12 |
| Figure 2.1 Simple Representation of Humid Air Exposure Box..... | 22 |
| Figure 2.2 Simple Sketch of the Process of Casting Corrugated Membranes | 23 |
| Figure 2.3 Structures of Dopamine (Left) and Polydopamine (Right) | 24 |
| Figure 2.4 Chemical Structure of Trizma HCl..... | 25 |
| Figure 2.5 Polydopamine Coating Process | 25 |
| Figure 2.6 Dimensions and Their Labels for a Corrugated Membrane | 26 |
| Figure 2.7 Membrane Module with 4.5 cm x 4 cm Active Area | 27 |
| Figure 2.8 Flowchart of the Crossflow Filtration System..... | 29 |
| Figure 3.1 Ternary Phase Diagram of A Casting Solution | 34 |
| Figure 3.2 Example of Membranes | 34 |
| Figure 3.3 SEM Images of PES Membrane Exposed to 0.9 L/min Humid Air (on the left) and 1.6 L/min Humid Air (on the right) with a Relative Humidity of 80% for 5 minutes | 36 |

| | |
|--|----|
| Figure 3.4 SEM Images of the Membrane Exposed to Humid Air for 4 Minutes, at 0.9 L/min Flow Rate with Relative Humidity of 80% | 40 |
| Figure 3.5 SEM Images of the Membrane Exposed to Humid Air for 3 Minutes, at 0.9 L/min Flow Rate with Relative Humidity of 80% | 41 |
| Figure 3.6 Cross Sections of Membranes Exposed to Different Relative Humidity for 5 Minutes | 43 |
| Figure 3.7 Cross Sectional SEM Images of Membranes Exposed to Humid Air with Relative Humidity of 50% for 10 minutes a) 0.9 L/min Humid Air Flow Rate b) 1.6 L/min Humid Air Flow Rate | 45 |
| Figure 3.8 Pure Water Permeance Values of the Membranes | 53 |
| Figure 3.9 FTIR Results of the Membranes..... | 54 |
| Figure 3.10 Surfaces of Coated and Uncoated Corrugated membranes a)Coated Corrugated Membrane b) Uncoated Corrugated Membrane | 55 |
| Figure 3.11 Closer Look Up on Surfaces of Coated and Non-Coated Membranes .. | 56 |
| Figure 3.12 Comparison of the Fouling Resistances of Uncoated Flat and Corrugated Membranes for Re=444 | 58 |
| Figure A.1 Comparison of P/PWP Values for Coated and Uncoated Flat and Corrugated Membranes for Re=444 | 69 |
| Figure B.1 TMP versus Permeate Flux of a Corrugated Membrane with a Pure Water Permeance Value of 224.18 L/m ² hbar | 72 |
| Figure C.1 Change of Retention and Permeance of a Polydopamine Coated Corrugated Membrane | 74 |

NOMENCLATURE

MF : Microfiltration
LIPS : Liquid Induced Phase Separation
VIPS: Vapor Induced Phase Separation
CFV : Cross Flow Velocity
 C_w : Concentration at the wall
 C_b : Bulk concentration
J : Permeate flux
 δ : Concentration polarization layer thickness
 R_{mem} : Retention of the membrane
D : Diffusivity of rejected component
TMP : Trans-membrane pressure
 μ : Viscosity of permeate stream
 R_{tot} : Total resistance to flow
 R_m : Membrane intrinsic resistance
 R_g : Resistance due to gel layer
 R_{cp} : Resistance due to concentration polarization
 R_p : Resistance due to pore blocking
 R_a : Resistance due to adsorption phenomena
Q : Volumetric flow rate read from rotameter
A : Area perpendicular to flow in membrane module
 Re : Reynolds number
 ρ : Density of the feed stream
 d_H : Hydraulic diameter
P : Wetted perimeter
PWP : Pure water permeance
TMP : Trans Membrane pressure difference
 R_{ff} : Final fouling resistance
 R_{fi} : Initial fouling resistance

PES : Polyethersulfone

PEG: Polyethylene glycol

NMP: N-methyl-2-pyrrolidone

CHAPTER 1

INTRODUCTION

1.1. Membranes and Filtration

Membrane can be defined as a semi permeable barrier that separates a mixture, by leaving the rejected components on the retentate side while rest of the mixture permeates through the membrane during a filtration process ^[1]. These selectively permeating synthetic structures are used in a variety of areas from fuel cells to water treatment, including areas like food industry and pharmaceutical applications. The main materials used in membranes for industrial applications and scientific research are polymers, despite the fact that there are membranes produced from materials like metals and ceramic ^[2]. Figure 1.1 shows a simple example of a membrane filtration process:

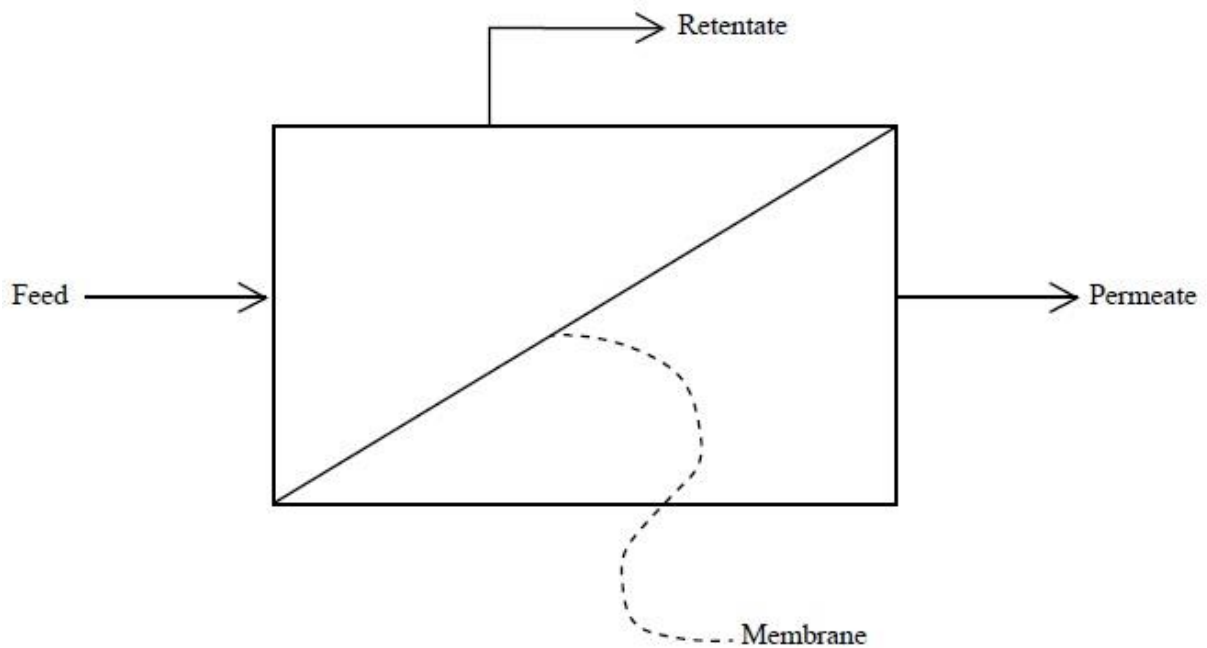


Figure 1.1: A Simple Drawing of a Membrane Filtration

The feed stream that comes to the membrane is divided into two streams; retentate, where the rejected components are collected, and permeate, where the permeated components pass through. Permeate volume per unit membrane area per unit time can be defined as the flux (J) of a membrane, and it is generally expressed in L/m^2h for liquid separation membranes. The flux through a membrane during the filtration process changes with the driving force, which is the trans membrane pressure, and this change is defined with the term permeance, that is usually expressed in L/m^2hbar .

Pressure driven membrane applications can be classified in four processes; microfiltration (where pore sizes vary between 10^{-1} and $10 \mu m$), ultrafiltration (where pore sizes vary between 1 and 100 nanometers), nanofiltration (where pore sizes vary between 1-2 nanometers) and reverse osmosis (where membranes are dense). The pressure driven membranes have a mechanism of transport by either solution diffusion or by pore flow. While the separation process in pore flow depends on the

pore size of the membrane as well as the size of the species, separation occurs by permeating through free volume, the volume that is not occupied by the molecules, of the membrane during solution diffusion ^[1].

Microfiltration is a separation process that uses pore flow transport mechanism, and membranes having pore sizes larger than 0.1 μm , in order to dissociate the suspended particles in a mixture. The polymeric membranes that are used in microfiltration can have symmetric structure, where there is a uniform pore size distribution throughout the membrane cross section, or asymmetric structure, where the pore sizes change throughout the cross section, morphologies depending on the production conditions. Asymmetric membranes are usually composed of a thin, dense skin layer that effectively causes the separation, and a thicker support layer that has larger pores and gives mechanical strength to the membrane. Figure 1.2 shows simple schematics of symmetric and asymmetric membranes:

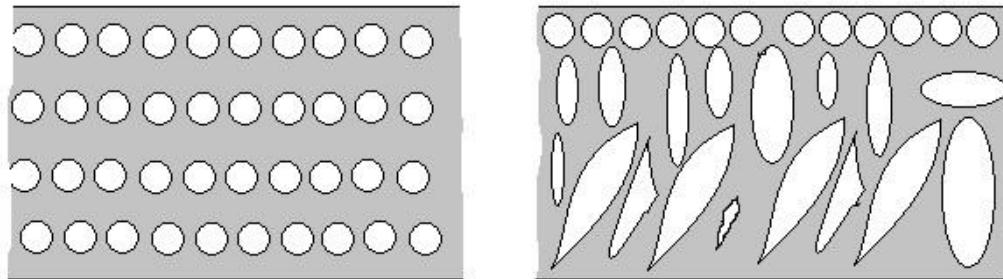


Figure 1.2: Simple Schematics of Symmetric and Asymmetric Membranes

1.2. Phase Separation Micro-Molding

One of the most used methods for the production of porous membranes from polymer solutions is the phase separation method. Phase separation methodology can be classified in three methods; non solvent induced phase separation (where coagulation is achieved via induction of either liquid or vapor non solvent), thermal gelation (where phase separation is achieved by cooling down a hot cast polymer

solution) and solvent evaporation (where the polymer solution is composed of more than one solvent, and evaporation of one solvent leads to a concentration change, resulting in precipitation) ^[1,3].

The one phase, usually liquid, polymer solution turns into a two phase mixture with the addition of non solvent during non solvent induced phase separation method. The matrix of the membrane is formed by solid, polymer rich phase of this mixture, while the porosity is introduced into the morphology by the liquid and polymer lean phase. Figure 1.3 shows an example of ternary phase diagram, representing the three components of a polymer solution during non solvent induced phase separation:

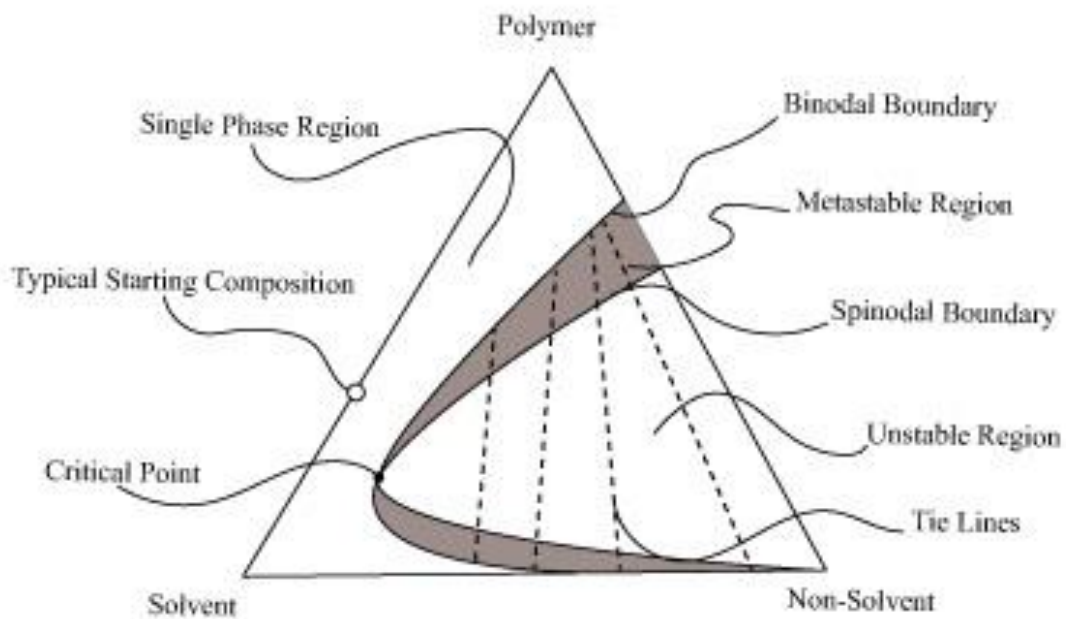


Figure 1.3: Ternary Phase Diagram Sample for a Non Solvent Induced Phase Separation Process

Each corner of the triangle represents pure components of a polymer mixture; a typical polymer solution starts on the solvent-polymer line, moving inside the

triangle as the non solvent is introduced. Binodal boundary shows the miscibility of the polymer solution components, separating one phase region from two phase. There is a chance that the solution does not immediately precipitate after passing the binodal curve, and the components can stand the small concentration changes within a region beyond the binodal boundary. This region is named the metastable region, the limit of which is called the spinodal boundary, and the solution becomes unstable after the spinodal boundary. Porosity is introduced into the membrane morphology during this path via nucleation and growth ^[4]. Critical point is the interception of binodal and spinodal boundaries; if the phase separation starts above the critical point, resulting matrix becomes polymer rich, vice versa results in a polymer lean matrix. The tie lines represent the connections between polymer rich and polymer lean phases that are on the binodal boundary ^[5].

Phase separation micro molding is a versatile, straightforward and cost effective microfabrication technique that can be applied to a wide range of polymers, relying on the phase separation of a polymer while in contact with a structured mold ^[6]. The non solvent commonly used during these processes is water, since it is cheap and easily available. The desired micro patterned membrane structure is usually achieved via induction of liquid, induction of vapor or a combination of both liquid induced and vapor induced phase separations. Figure 1.4 shows a typical phase separation micro molding process:

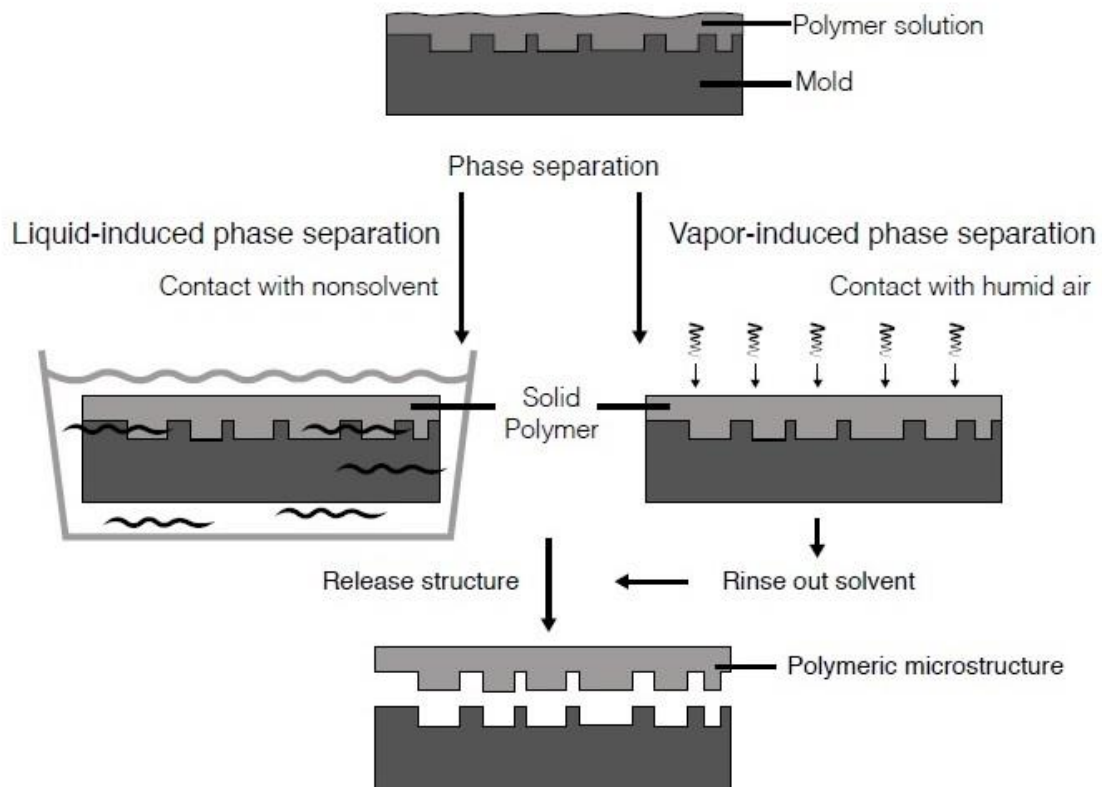


Figure 1.4: A Typical Phase Separation Micro Molding Process

Exposing the cast polymer solution to non solvent vapor prior to coagulation results in reduced number of macro voids and a thinner skin layer ^[7, 8]. Since a thinner skin layer is desired for a faster filtration, and it was aimed to introduce a skin layer on the mold side of the membranes, a combination of vapor induced phase separation and liquid induced phase separation is used to produce polymeric membranes from polyethersulfone in this study.

1.3. Factors Affecting Membrane Performances

Membrane processes deal with two main problems regarding the issue of membrane performances.

Concentration polarization, being the first of these problems, is the mass transfer boundary layer caused by the rejected materials on the feed side and near the

membrane wall during filtration. Resulting in a concentrated layer of rejected materials near the surface, concentration polarization causes a decrease in the concentration difference of permeating species between the two sides of the membrane, which in turn leads to a decrease in flux and selectivity^[9]. Moreover, the cost of filtration inclines due to concentration polarization, because the concentrated layer of rejected materials causes an extra resistance on the filtration process. A simple drawing of concentration polarization is shown in Figure 1.5:

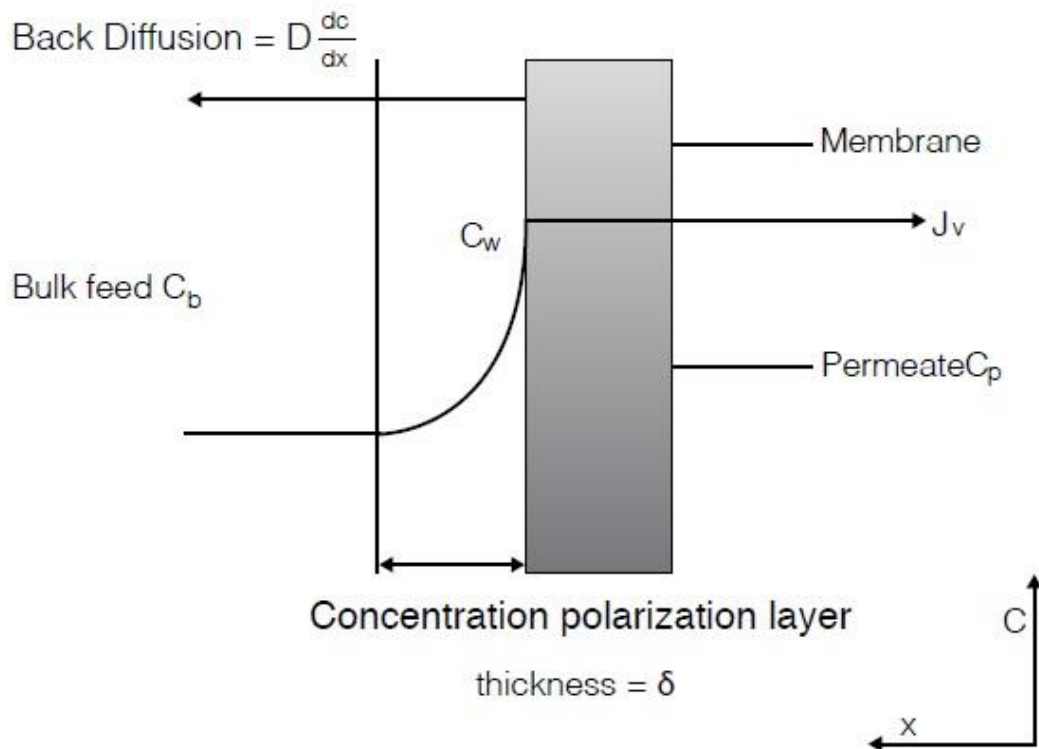


Figure 1.5: Simple Representation of Concentration Polarization

Concentration polarization and its influence on the filtration process is often expressed by the term concentration polarization modulus C_w/C_b :

$$\frac{C_w}{C_b} = \frac{\exp\left[\frac{J\delta}{D}\right]}{\exp\left[\frac{J\delta}{D}\right] - R_{mem} \left[\exp\left[\frac{J\delta}{D}\right] - 1\right]}$$

Which reduces to the equation below for 100% rejection:

$$\frac{C_w}{C_b} = \exp \left[\frac{J\delta}{D} \right]$$

Where C_w and C_b indicate the concentrations on the wall and of the bulk, respectively. While δ symbolizes the concentration polarization layer thickness, J shows the permeate flux. R_{mem} is the rejection of the membrane to the species and D indicates the diffusivity. When the wall concentration is equal to the concentration of the bulk, meaning concentration polarization modulus is equal to 1, it means there is no concentration polarization in the process.

Membrane fouling is the accumulation of rejected components on the surface and inside the pores of the membrane. This accumulation may lead to a decrease in the pore sizes throughout the membrane cross section, cake formation on the membrane wall and as a result, a decrease in the permeate flux, or an increase in trans membrane pressure for the membranes that are used in pressure driven processes. Fouling also leads to an increase in energy use during the process. In addition, if the fouling is irreversible, it decreases the life span of the membrane. Therefore membrane fouling remains a vital hindrance for the filtration processes. The flux on a membrane surface can be defined by Darcy's Law:

$$J = \frac{TMP}{\mu(R_{tot})}$$

Where TMP implies the trans membrane pressure, μ is the permeate stream viscosity and R_{tot} is the total resistance to flow. These resistances can be summarized with Figure 1.6:

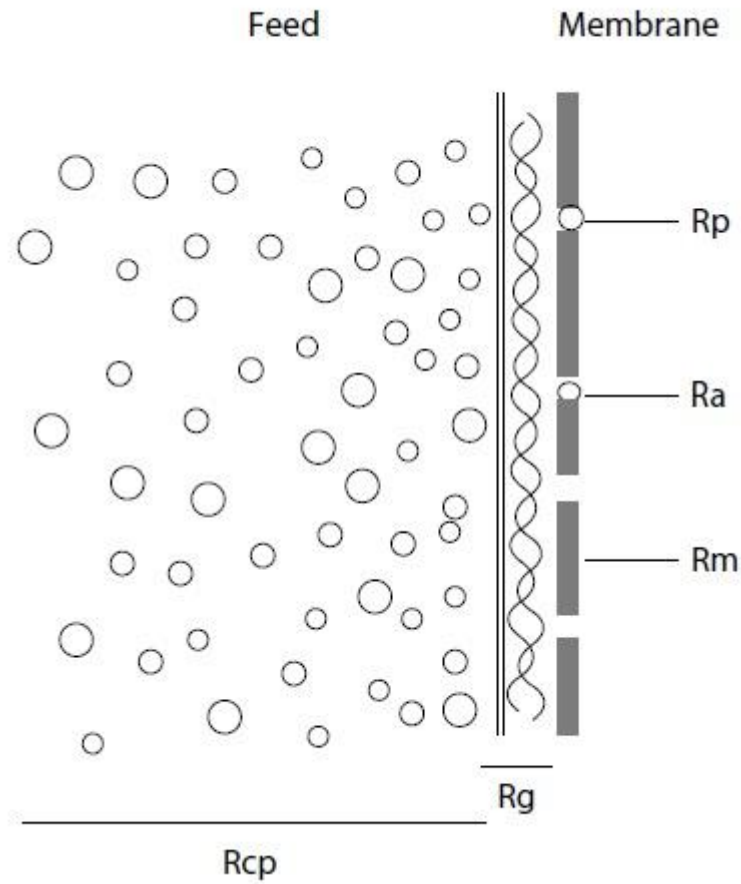


Figure 1.6: Representation of Flow Resistances During Filtration

R_m indicates the intrinsic resistance of the membrane, which should be the only factor in the total resistance for case of no concentration polarization and fouling. The rejected materials may result in a gel layer on the membrane surface as explained above, the resistance of which is expressed as R_g in the figure. R_{cp} is the resistance caused by concentration polarization, which causes a concentration gradient decrease during the process. While R_a is the resistance caused by absorption^[2], R_p is the resistance resulting from the size reduction and blocking of the pores due to fouling.

1.4. Preventing the Effects of Concentration Polarization and Fouling

There are a variety of methods that can be applied to reduce, if not totally prevent, the effects of concentration polarization and fouling during membrane filtration processes. These methods can be classified into three; feed modifications, surface modifications and changing the flow hydrodynamics ^[10, 11].

Feed modifications can be done prior to filtration; coagulation, pre treatment, flocculation and absorption are a number of suggested methods for feed modification. Al-Malack and Anderson studied the influence of flocculation as pre treatment on microfiltration membranes, and they have added alum to bio treated sewage effluents to find out that it increases the flux. They underlined that this result can be imputed to agglomerated particles, by adding that they can be taken off easily by shearing ^[12]. Abdessemed and coworkers presented that adsorption could be an effective pre treatment method for removing effluent organic matter on both microfiltration and ultrafiltration membranes, and flocculation improves the permeate flux ^[13]. Howe et al. investigated the interactions between water quality, coagulation and membrane fouling by examining the fouling of microfiltration and ultrafiltration membranes with natural water and its ingredients. They found out that coagulation, as a pre treatment method, has a primary impact on the filtration for the materials with fractions of 1 μm and 100 kDa in size ^[14].

Surface modifications on a membrane can hinder the effect of fouling by decreasing the absorption, or making the membrane easier to clean. Reddy et al. studied the effects of using poly sodium styrene sulfonate on polyethersulfone (PES) ultrafiltration membranes, and they have observed that the flux decreases for polyethylene glycol (PEG) and dextrans for the surface modified membranes. They underlined that the surface modified membranes demonstrate better anti fouling properties when compared to their unmodified counterparts ^[15]. Ma and coworkers proposed a new method for PES ultrafiltration membranes; they modified the surfaces of the membranes with polyvinyl alcohol and borax solution by using adsorption-crosslinking cycles, and performed fouling tests using bovine serum albumin (BSA) solutions to conclude that the surface modified membranes have

enhanced hydrophilicity in addition to acceptable reduced fluxes during filtration ^[16]. Galjaard et al. coated the surfaces of PES ultrafiltration membranes with bentonite, diatomite, iron oxide, kaolinite, titanium dioxide, zeolite and like materials. They treated the surface water from Twente canal, lake and reservoir to observe that despite having a higher fouling rate as a result of precoating, the membrane performances stabilize after several filtration cycles ^[17]. Mu and Zhao used a thermally induced surface cross linking process to coat the surfaces of PES membranes with polyethylene glycol diacrylate and trimethylolpropane trimethylacrylate; they showed that the modified membranes were less prone to fouling when compared to the unmodified ones, in addition to having improved flux recoveries after cleaning, during BSA filtration ^[18]. King et al. have applied ion beam irradiation to commercial polyethersulfone membranes and treated them with natural organic matter; they have observed that the irradiation resulted in a diminution in the charge of the membrane, as well as the fouling becoming reversible after the modification ^[19]. Kull et al. applied nitrogen containing plasma treatment to PES membranes; using different plasma gases like N₂, NH₃, O₂/NH₃ and Ar/NH₃ to find out that the modified membranes had lower fouling when compared to the unmodified ones. In addition, they have discovered that the modification results in an enhanced water flux as well as a significant flux recovery after gentle cleaning ^[20]. Wavhal and Fisher applied argon plasma treatment to PES membranes and they came across with a dramatic increase in the pure water flux of these membranes after the treatment. Moreover, they noticed that the modified membranes were easier to clean, requiring less caustic for permeation flux recovery ^[21]. Wang et al. synthesized novel branched amphiphilic copolymers using polyethylene glycol with the molecular weight of 400 kDa and Pluronic P123, and blended these copolymers to the casting solution with PES to produce ultrafiltration membranes. The membranes were observed to have higher resistance to protein adsorption, reversible fouling during ultrafiltration and much better flux recovery ratios when compared to their unmodified counterparts ^[22]. Rahimpour et al. added poly(amide imide) to the casting solutions with PES and produced ultrafiltration membranes for milk-water filtration. Modified membranes have shown higher flux and better antifouling behavior as well as higher surface and sublayer porosity ^[23]. The variety of surface modification

methods and their results prove that surface modification is an applicable method for increasing surface hydrophilicity, which in turn improves the anti fouling behavior of the membranes.

Changing the flow hydrodynamics may play an important role while dealing with the effects of concentration polarization and fouling, and it can be achieved via a variety of methods; applying cross flow instead of dead end filtration in order to clean up the foulants that may build up on the membrane walls, and introducing patterns to the membrane surface in order to promote turbulences and eddies are the common examples ^[24]. This study focused on introducing patterns, corrugations specifically, on the membrane surface and used cross flow filtration method instead of dead end filtration.

1.5. Patterned Membranes

Introducing patterns on the membrane surface increases the surface area, promotes turbulence and therefore increases flux while decreasing the effects of fouling. Since the beginning of 2000's, research on surface modification of membranes in order to mitigate fouling and enhance permeation has a demanding increase, and a variety of valuable work has been done on the matter. Figure 1.7 represents how corrugations may affect the flow around the membrane surface by introducing local turbulences:



Figure 1.7: Representation of Corrugations on the Flow

Scott et al. mechanically pressed polytetrafluoroethylene (PTFE) and polyvinylidene fluoride (PVDF) membranes at 120 °C to get corrugations, and these corrugated

membranes were compared with flat ones; they have decided that corrugations decrease concentration polarization and enhance flux by 30 %, 100 % and 160 % for parallel, 45° and 90° corrugations respectively. In addition, they have seen that energy consumption decreases by 80 % and 88 % for 45° and 90° corrugations respectively. They finally concluded that use of corrugations is more effective than increasing cross flow velocity ^[11].

Zhang and co-workers tried to model the transport of water vapor in dry air by using cross-corrugated membranes, and they have found two correlations for friction factor and Sherwood number; the experiments resulted in corrugations increasing the complexity of flow pattern, separation, recirculation and reattachment. Moreover, the results showed that increasing Reynolds number moves the turbulence center from lower regions of corrugations to upper regions ^[25].

Hu et al. tried to explain the influence of membrane material, process conditions and corrugation on emulsion microfiltration in 2007 to find out that use of corrugations increase flux rate at same conditions when compared to flat membranes. They have used 2 mm wide and 1 mm high sinusoidal corrugations, while for fouling they have used water-oil emulsion. In the results, they have seen that 90° corrugation increases the steady state flux 3.3 times and effective membrane area was increased by 45 % ^[26].

Maruf et al. proposed nanoimprint lithography technique to produce sub-micron patterns on polysulfone membranes in 2013. They have patterned flat membranes at 120 °C and 4 MPa for 180 seconds. Similar to others, they have concluded that surface patterns minimize particle deposition and total cake resistance, while they increase critical flux. In addition they observed a highly anisotropic particle deposition on surface, and this deposition decreased with increase on the orientation angle between pattern lines and feed flow direction ^[27].

Elimelech et al. have conducted laboratory scale colloidal fouling tests on cellulose acetate and aromatic polyamide thin film composite reverse osmosis membranes in order to compare their fouling performances. They found out that the composite membranes exhibit significantly higher fouling rates. This behavior was attributed to

their surface roughness that is naturally formed during interfacial polymerization of aromatic polyamide membranes, and this conclusion was supported by comparing the AFM and SEM images of two membranes ^[28].

Gohari et al. have studied the effect of patterns on fouling of membranes and controlling the patterns during phase separation. They concluded that the reason Elimelech et al. observed an increase in fouling while patterned membranes were used ^[28] was because these patterns were not aligned. They observed that pattern formation can be controlled by controlling the filler amount, fouling can be decreased by using perpendicular flow to patterns and washing is easier with parallel-to-patterns flow ^[29].

Won et al. have published a variety of papers on patterned membranes. They prepared PVDF membranes with DMF and acetone by using phase separation micro-molding. In 2012, they have investigated the differences between flat, prism corrugated and pyramid corrugated membranes to conclude that increasing PVDF amount decreases the pattern fidelity for prism patterned membranes and that minimum amount of PVDF might be necessary to avoid defects. Thicknesses of all membranes were the same and patterning did not significantly affect pore sizes ^[24].

The same year Won and coworkers published another article on analyzing the flow and fouling on membrane surfaces with the same membrane solutions. They have used CFD for flow analysis to conclude that vortices were formed in the lower region of patterns, local shear stress was higher at the upper region and there was more fouling on the lower region when compared to upper region ^[30].

In their paper in 2014 on factors affecting pattern fidelity and performance of a patterned membrane Won et al. have defined pattern fidelity, measurement of how similar the dimensions of the membrane to the patterned mold, as in the equation below:

$$\text{Fidelity of a Dimension} = \frac{\text{Measurement of the Dimension on the Membrane}}{\text{Measurement of the Dimension on the Mold}}$$

They have concluded that increasing polymer molecular weight decreases phase inversion rate and fidelity, and the morphology goes from finger-like structure to sponge-like structure. On the other hand, they have observed that fidelity decrease is not as severe with increasing molecular weight, when the polymer concentration increases. They also observed that increasing pattern height increases water flux and surface area, while decreasing microbial attachment ^[31].

Maruf et al. investigated the effects of substrate topography and interfacial polymerization conditions on fabrication of surface patterned thin film composite membranes in 2016, by producing thin film composite membranes with patterns of different heights but same periodicities. They have observed that nanoimprint lithography can be used to control the topography of the support for a patterned membrane, which results in an ability to control the membrane topography when combined with the tuning of chemistry and kinetics of interfacial polymerization during the process ^[32].

Elsherbiny and coworkers have produced polyamide thin film composite membranes with micro patterns via combining vapor induced phase separation and non-solvent induced phase separation micro molding techniques, to examine the permeances and fouling behaviors of these membranes using sodium chloride solution ^[33]. In addition, they introduced a simplified and cost effective method for imprinting flat PES membranes for the first time. They have oriented the micro patterned channels both parallel and perpendicular to the feed flow, and observed that parallel orientation results in an increase in the efficiency of mixing and eddies on the surface, which in turn diminishes the effects of concentration polarization. Moreover, the study attributes the enhanced permeability of patterned membranes to increased surface area and improved membrane surface roughness.

1.6. Polydopamine Coating

Common foulants like proteins, emulsified oils and microorganisms usually have more tendency for adhesion to hydrophobic membrane surfaces when compared to hydrophilic membrane surfaces ^[34]. Hydrophilic surfaces are theorized to result in a bond of tight layer of water, decreasing the foulant deposition coming from aqueous

media, therefore reducing the hydrophobic-hydrophobic forces between the membrane and foulant ^[35]. As a result, most of the surface modification studies focus on increasing the hydrophilic properties of membrane surfaces ^[36], as reported in the previous sections.

Polydopamine coating on porous membrane surfaces have an increasing demand since Messersmith and coworkers have proposed an easily applicable method inspired by mussels to deposit polydopamine on a variety of materials from metals to synthetic polymers in 2007. They reported that polydopamine can easily be deposited homogenously on corrugated surfaces as well, via an aqueous buffer solution, and the coating increases the hydrophilicity of the surface ^[37]. Since mussels need to overcome the effects of hydration and remove the weak boundary layers in order to secure contact with bare surfaces, they have taken interest of biomimetic scientists. Dopamine and polydopamine were shown to mimic the adhesion mechanisms of mussels such as intrinsic protein binding and covalent coupling, therefore can mimic the adhesive behavior of mussels under specific pH conditions ^[38]. In addition, being done under mild and aqueous conditions, polydopamine coating is a great alternative when compared to other coating methods since it does not require drying and does not result in a degradation of the polymer on which polydopamine is deposited. Moreover, permeability of the membranes can be changed by controlling the polydopamine layer thickness on them, which can be achieved by varying the coating time or dopamine concentration in solution ^[34].

McCloskey et al. conducted polydopamine coating on polysulfone ultrafiltration membranes, polyvinylidene fluoride microfiltration membranes and polyamide reverse osmosis membranes to observe its effect on their pure water fluxes and BSA rejections during dead end filtration. They have coated the membranes using a Tris buffer solution containing 2 mg/mL dopamine. They observed that BSA adhesion was decreased on the coated membranes. In addition they have underlined that the polydopamine coated porous membranes, meaning microfiltration and ultrafiltration membranes, show a decreased pure water flux when compared to their uncoated counterparts. They affiliated these results with the related pore sizes of those membranes; microfiltration membranes had smallest pure water flux decrease,

around 1%, since they had larger pores while ultrafiltration membranes showed a decrease up to 40% and reverse osmosis membranes had a decrease of 25% after 90 minutes of coating ^[39].

Zhu et al. have prepared porous polyethylene membranes with pore sizes of 0.5 μm using stretching method in 2010, and modified their surfaces using a Tris/HCl buffer solution with a pH of 8.5, containing 2 g/L dopamine. The membranes were rinsed with deionized water and ethanol, after being immersed and shaken in the buffer solution for 24 hours. The effects of coating were tested using FTIR, XPS and for their pure water permeances. While the contact angles of the membranes decreased from 114° to 43°, the FTIR results showed peaks around 1610 m^{-1} and pure water permeances have increased from 370 to 644 $\text{L}/\text{m}^2\text{hbar}$ ^[40].

Cheng and coworkers have dissolved 2 mg/mL dopamine in a phosphate buffered saline solution with an 8.5 pH, immersed polyethersulfone ultrafiltration membranes in this solution and shaken for different time spans in 2012, the coated membranes were then rinsed with double distilled water for 24 hours. The contact angle of 74° that the uncoated membranes had decreased to 67°, 60°, 58° and 55° for 2, 4, 8 and 24 hours of coating respectively. On the other hand, FTIR results have given peaks around 1610 and 3400, indicating the signs of polydopamine coating. While the pure water flux decreased to almost zero after a few hours of coating, it was stated that the flux could be tuned between 10 and 200 $\text{mL}/\text{m}^2\text{hmmHg}$. In addition, the coated membranes reported to have higher PBS fluxes and they were finally tested for their bovine serum albumin (BSA) rejection performances, to observe that there is not any significant difference between them ^[41].

Li et al. have prepared a buffer solution with a pH value of 8.8 from tris, and then dissolved 80 mg/mL dopamine in this solution. They have rinsed polyethersulfone ultrafiltration membranes having molecular weight cutoff between 6 and 20 kDa in this solution and shaken for 1 hour, after the rinsing they have washed the membranes with ethanol and distilled water. They reported a decrease in the contact angles of the membranes after coating, and peaks around 1660 at FTIR analyses. They wetted the membranes in isopropanol for an hour and compacted them before

applying dead end filtration to the coated and uncoated membranes to observe that the flux decreased after coating. Li and coworkers underlined this result and associated the significant decrease of flux in membranes having 20 kDa molecular weight cutoff due to their larger pore size distribution ^[42].

Yang and coworkers have also studied polydopamine coating in 2014, on polypropylene microfiltration membranes having 0.2 μm mean pore size with 75% porosity. They have coated the membranes using 2 mg/mL dopamine solution in a tris buffer having 8.5 pH. The membranes were wetted in ethanol prior to coating, shaken during the process, washed three times and dried at 40°C after coating. Once again peaks were observed around 1600 during FTIR analyses and membranes were then tested for their permeabilities. While the 2 hours coating have not changed the permeability significantly, there was an increase for 4 and 6 hours coating. The 4 hour coated membranes had an increase of 2730 L/m²h, while the permeability of 6 hour coated membranes increased 6796 L/m²h ^[43].

Miller, Kasemset, Wang, Paul and Freeman have evaluated the performance of polydopamine and polydopamine grafted polyethylene glycol coatings on polysulfone ultrafiltration membranes during constant flux cross flow filtration in 2014. They coated the membranes using 2 mg/mL dopamine containing tris buffer solution with a pH of 8.8. The modified and unmodified membranes were then exposed to soybean oil at six different flux values to find out that despite having similar pure water flux values, the modified membranes perform with a lower trans membrane pressure above the threshold flux. On the other hand, the modified membranes exhibited higher trans membrane pressure below the threshold flux, which was related to the decrease on their permeabilities after coating. At the end of their study, Miller and coworkers have underlined the fact that membranes of higher permeabilities can be modified via polydopamine and polydopamine grafted polyethylene glycol in order to increase the fouling resistance while keeping the other membrane properties constant ^[44].

This study focused on polydopamine coating of flat and corrugated polyethersulfone microfiltration membranes in order to reduce their pore sizes, compare their fouling behaviors with their uncoated counterparts.

1.7. Aim of the Study

In order to tune the morphologies of microfiltration membranes produced via phase separation micro molding; factors affecting phase inversion and surface modifications were investigated throughout this study, and the study followed two main paths.

The first path was observing factors affecting the morphologies of membranes during phase separation micro molding, as flat and corrugated membranes were aimed to be compared for their performances during cross flow yeast filtration. For this purpose, membranes were produced using polymer solutions composed of polyethersulfone as main polymer matrix, N-methyl-2-pyrrolidone (NMP) as solvent, water as non-solvent and polyethylene glycol (PEG 400) as pore forming additive. It was aimed to introduce an inverse asymmetric structure to the membrane morphologies by changing relative humidity, humid air exposure time and humid air flow rate during membrane production.

The second path was examining the effects of polydopamine coating on flat and corrugated membranes and their performances, again during cross flow yeast filtration.

CHAPTER 2

EXPERIMENTAL METHODS

2.1. Materials

Polyethersulfone is frequently preferred for the production of microfiltration and ultrafiltration membranes due to its good chemical resistance, thermal stability, mechanical and film forming properties ^[39]. Therefore polyethersulfone (Ultrason E2060P) was chosen as the main polymer matrix, provided by BASF, and kept in an oven at 80°C for at least a day before use. N-methyl pyrrolidone (NMP with purity of 99%) was chosen as the solvent and was obtained from Sigma-Aldrich. Polyethylene glycol (PEG 400) was chosen as an additive and pore forming agent, and was obtained from Sigma-Aldrich. The non-solvent of the polymer solution was ultrapure water with a conductivity value of 18.2 $\mu\Omega$.cm, and the cast solution was coagulated in distilled water. Dopamine hydrochloride (99%) that is used for polydopamine coating was purchased from Alfa Aesar, and Trizma HCl used for preparing the buffer solution was purchased from Sigma Aldrich. Commercial yeast (Dr. Oetker) was obtained from a local store for yeast fouling tests.

2.2. Membrane Casting

2.2.1. Solution Preparation

A variety of solutions were tried to be prepared in order to decide on which solution to work with. It was decided to continue with the solution in which 10% PES was

dissolved in a mixture of 25% NMP, 60% PEG 400 and 5% water by weight. The solutions were prepared, stirred and kept at room temperature.

2.2.2. Flat Membranes

The polymer solution was poured onto a silicon wafer, and the film was formed by casting with a stainless steel casting bar having a uniform thickness of 250 μm . The wafer with the cast solution on it was then taken to a humid air exposure box at 80% relative humidity that is introduced by passing air through water at 50°C in order to move on with vapor induced phase separation, and kept there for various time spans. Figure 2.1 shows a simple representation of the humid air exposure box:

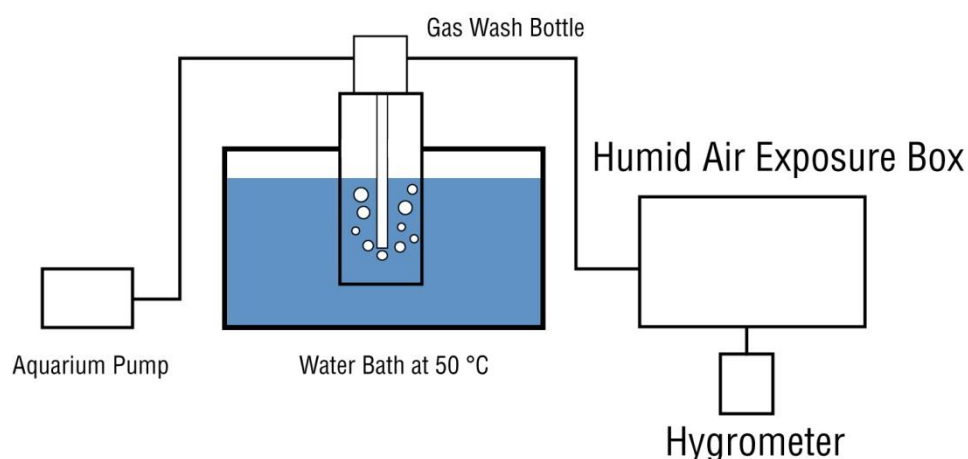


Figure 2.1: Simple Representation of Humid Air Exposure Box

After the related time is passed, the wafer was put into a distilled water bath at room temperature in order to proceed with liquid induced phase separation and complete the coagulation, and kept there for 15 minutes. Finally, the cast membrane is detached from silicon wafer and put into a distilled water bath, the membrane is kept in the bath overnight before it was put into ethanol bath. Membranes were put in an ethanol bath for 2 hours before drying in order to reduce the Laplace Pressure on the

pores, which results in the prevention of pore collapsing. Laplace Pressure is defined as the pressure difference between the inside and the outside of a curved surface forming a boundary between two phases, and can be expressed using Young-Laplace Equation given below:

$$\Delta P = \frac{2\gamma\cos\Theta}{a}$$

Where ΔP is the pressure difference across the fluid interface, γ is the surface tension, Θ is the contact angle and a is the capillary radius. After being dried from ethanol, flat membranes were ready for the performance tests.

2.2.3. Corrugated Membranes

The corrugated membranes were produced using almost the same methods as the flat membranes. The only difference, however, was the mold used during casting; the membranes were cast on a corrugated silicon wafer that is produced via deep reactive-ion etching (DRIE) method, that enables the microfabrication of high aspect ratio structures in silicon, in METU-BIOMEMS center. DRIE method is composed of cycles that are repetitive alternations of plasma etch (vertically attacking ions, SF_6 usually for silicon) and an inert passivation layer deposition. While the plasma etch step carves the desired microstructure on the silicon mold by bombarding with ions, passivation step deposits a layer on the carved surface to stop further etching by ions and this cycle results in a high aspect ratio as well as a very directional etch and sidewalls with good surface planarity for corrugations ^[45]. Figure 2.2 shows a simple sketch of the casting process:

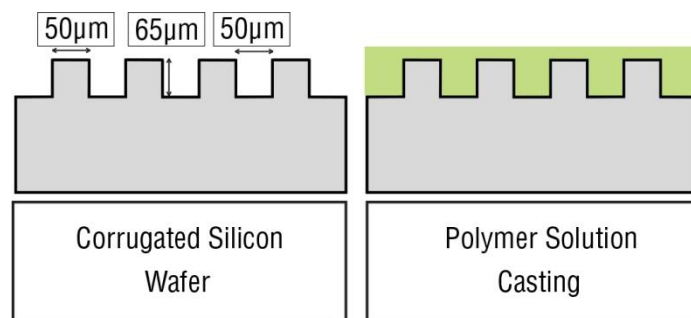


Figure 2.2: Simple Sketch of the Process of Casting Corrugated Membranes

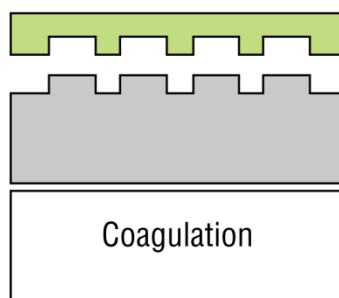


Figure 2.2 cont'd: Simple Sketch of the Process of Casting Corrugated Membranes

After casting and coagulation, corrugated membranes were exposed to the same procedure as the flat membranes for water bath and being dried from ethanol.

2.3. Polydopamine Coating

The cast membranes were coated with polydopamine for pore size tuning and comparison of the performances of coated and uncoated membranes. Dopamine was polymerized on the membranes using oxidative polymerization, where the reaction readily takes place when dopamine is treated in a basic environment. Figure 2.3 shows the structures of dopamine and polydopamine:

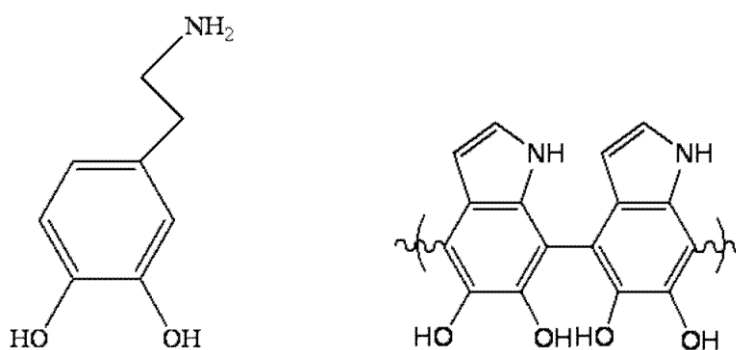


Figure 2.3: Structures of Dopamine (Left) and Polydopamine (Right)

The membranes that are tested for their pure water permeances were taken for polydopamine coating without drying them. Tris buffer with a pH of 8.5 was prepared using trizma HCl, which is used for introducing the basic environment for the polymerization to start and the chemical structure of which is given in Figure 2.4

below, and 2 mg/mL dopamine was put into the buffer solution as described by Messersmith and colleagues [35]:

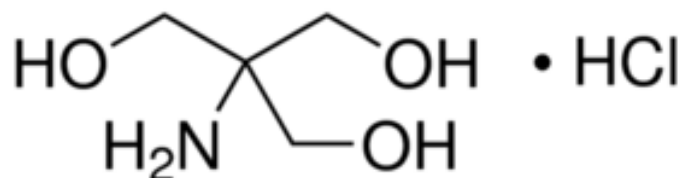


Figure 2.4: Chemical Structure of Trizma HCl

The membrane was put into this solution and started to be shaken gently, in order to start polymerization and coat the membrane surface with polydopamine. Figure 2.5 represents the coating process:

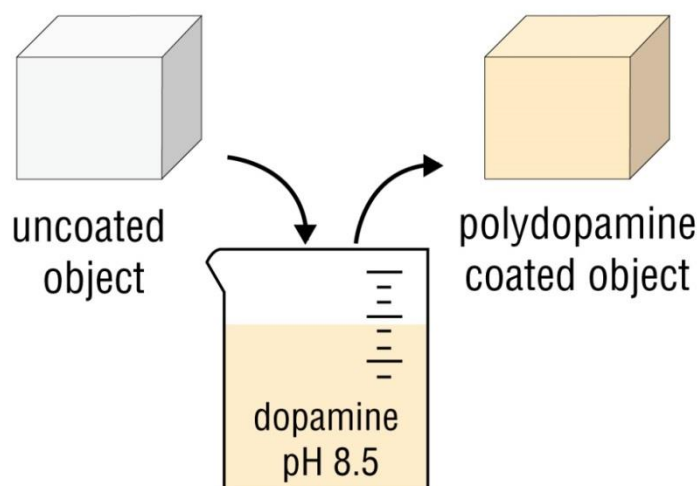


Figure 2.5: Polydopamine Coating Process

Membranes were kept in the solution while being rotationally shaken for 24 hours, and then washed three times in ultrapure water bath. Finally, at the third wash, the membranes were kept in the waterbath overnight; the washed membranes were taken to performance tests without drying, again in order to prevent the collapsing of the pores.

2.4. Performance and Morphology Observations

2.4.1. Morphology and Characterization

Membranes were examined using scanning electron microscopy (SEM, FEI Quanta-400 F) in METU Central Laboratory, in order to observe their morphologies, measure their thicknesses and determine their pore sizes. ImageJ software was used for the measurements; membrane thicknesses, dimensions of corrugations, distances between corrugations, porosity and pore connectivity were measured and analyzed. The membranes were broken in liquid nitrogen for the cross sectional analysis, kept under vacuum overnight, coated with palladium/gold particles in order to have a conducting layer before being analyzed with scanning electron microscopy.

Height and width fidelities of the corrugated membranes were calculated as defined by Won and coworkers' study^[31] and shrinkage on the corrugations was determined according to fidelity calculations:

$$\text{Fidelity of a Dimension} = \frac{\text{Measurement of the Dimension on the Membrane}}{\text{Measurement of the Dimension on the Mold}}$$

Dimensions were labeled as shown in Figure 2.4 below:

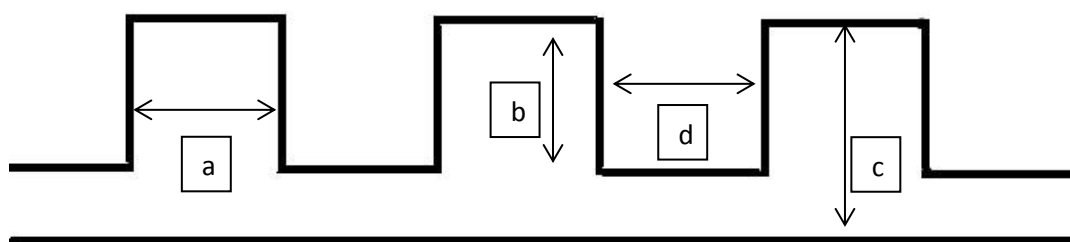


Figure 2.6: Dimensions and Their Labels for a Corrugated Membrane

Moreover, shrinkage on the membranes was defined as it was defined by Gençal et al. ^[10]:

$$S_{N+} = 1 - \frac{c (\mu m)}{315 (\mu m)} \quad S_{N-} = 1 - \frac{(c - b)(\mu m)}{250 (\mu m)} \quad S_N = 1 - \frac{t (\mu m)}{250 (\mu m)}$$

Where S_{N+} is the normal shrinkage of positive features and S_{N-} is the normal shrinkage of negative features for corrugated membranes; S_N is the normal shrinkage and t is the thickness for flat membranes. The lateral shrinkage for the corrugated membranes was defined as:

$$S_L = 1 - \frac{(a + d) (\mu m)}{100 (\mu m)}$$

This study shows the selective sides of the membranes on top in the SEM images; since skin layer forms at the non-solvent side for flat membranes, it is shown on top for the flat membranes while the mold side is shown on top since it is the selective side for corrugated membranes.

2.4.2. Pure Water Permeance Tests

Cross flow filtration method with a membrane module having 4.5 cm x 4 cm active area was used for permeating ultrapure water, bovine serum albumin (BSA) solution and yeast dispersion through the membrane in this study. Figure 2.6 shows this membrane module:

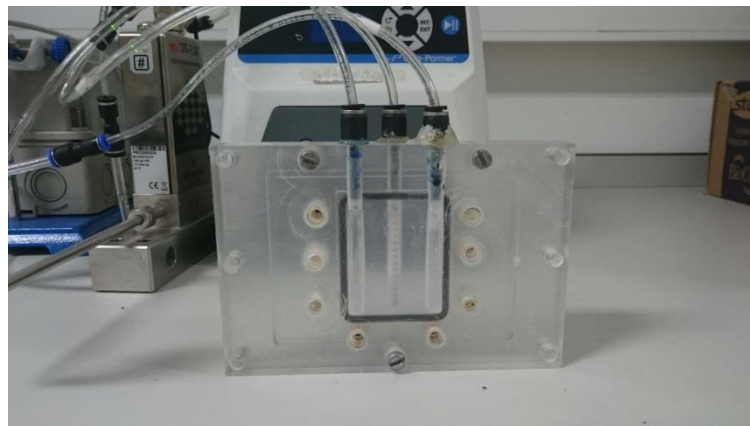


Figure 2.7: Membrane Module with 4.5 cm x 4 cm Active Area

Ultrapure water was pumped with a cross flow velocity of 0.063 m/s and a Reynolds Number of 136 during pure water permeance tests, and the tests were conducted under constant trans membrane pressure values of 1, 0.75, 0.50 and 0.25 bar. Cross flow velocity was calculated using the equation below:

$$\text{Cross Flow Velocity} = \frac{Q}{A}$$

Where Q represents the volumetric flow rate in m³/s and A represents the area perpendicular to the flow in m².

Reynolds Number was then calculated using the cross flow velocity:

$$Re = \frac{DV\rho}{\mu}$$

Where Re represents the Reynolds Number, D implies the hydraulic diameter of the flow in meters, V is the cross-flow velocity in m/s, ρ is the feed stream density in kg/m³ and μ is the viscosity of the feed.

Hydraulic diameter, on the other hand, was calculated using the equation below:

$$D_h = \frac{4A}{P}$$

Where A represents the cross sectional area for the flow in m² and P is the wetted perimeter in meters.

Figure 2.5 shows the flowchart of the cross flow filtration system:

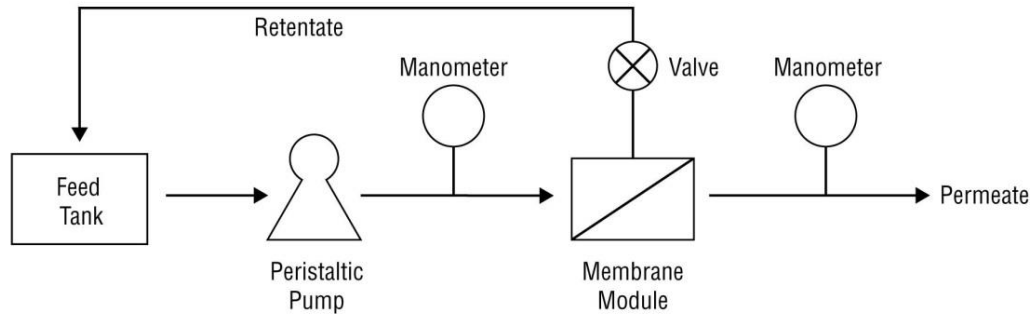


Figure 2.8: Flowchart of the Crossflow Filtration System

Trans membrane pressure was measured using a manometer on the feed stream and another on the permeate stream, and it was controlled using a valve in the retentate stream. Both permeate and retentate systems were recycled back to the feed system, while the flow rate of the permeate system was measured every 15 minutes until it reaches to steady state for every pressure value.

Pure water permeance of the membranes was calculated using the equation below:

$$PWP = \frac{J}{TMP}$$

Where PWP is the pure water permeance in L/m^2hbar , J is the flux in L/m^2h on membrane area and TMP is the trans membrane pressure in bar.

The steady state permeate flux at each pressure was taken, and a permeate flux versus pressure graph was plotted for each membrane, slope of which gave the pure water permeance of the membrane.

Using the pure water flux value and Darcy's Law, intrinsic resistance of the membrane to the flow was also calculated:

$$J = \frac{TMP}{\mu \times R_m}$$

Where J is the flux in L/m^2h , TMP is the trans membrane pressure in bar, μ is the permeate viscosity and R_m is the intrinsic flow resistance of the membrane in m^{-1} .

2.4.3. BSA Rejection Tests

BSA rejections of the coated and uncoated flat and corrugated membranes were tested in the study, using the same cross flow filtration set-up, in which the feed stream was composed of a 1 g/L BSA solution instead of ultrapure water and stirred at 250 rpm during the process in order to see whether the polydopamine coating had reduced the pore size and affected the BSA rejections. Five permeate samples of 5 mL were taken into tubes and their absorbance values were measured using UV/visible spectroscopy with UV-1601. These absorbance values were transformed into concentration with the calibration information obtained, and the percent BSA retentions of the membranes were calculated using the equation below:

$$\% \text{ Retention} = \left(1 - \frac{C_p}{\left(\frac{C_f + C_r}{2}\right)}\right) \times 100$$

Where C_f is the feed concentration, C_p is the permeate concentration and C_r is the retentate concentration.

Calculating also the permeance during filtration for each sample, a graph of permeance and percent retention versus permeate volume was plotted for each membrane.

2.4.4. Yeast Fouling Tests

Yeast fouling tests were also conducted in the same cross flow filtration set-up, with 0.025 weight percent dyed yeast dispersion in the feed tank instead of ultrapure water stirred at 250 rpm.

1 gram Dr. Oetker yeast was dispersed in 250 mL ultrapure water and centrifuged three times at 2500 rpm for 10 minutes. Precipitated yeast was then dried and dispersed in a solution composed of 0.15 g brilliant blue dye, 25 mL acetic acid, 62.5 mL isopropanol and 161.5 mL ultrapure water. The dispersion was stirred for a day, and then again centrifuged three times at 2500 rpm for 10 minutes, precipitated components were redispersed in ultrapure water after decanting the supernatant for the last two centrifuges. After the centrifuge process, the dyed and precipitated yeast

was once again dried. 400 gram of 0.025 weight percent yeast dispersion was used for yeast fouling tests.

The yeast fouling tests were applied to flat and corrugated membranes with and without coating at a constant pressure of 1 bar. The Reynolds numbers during filtration were chosen as 444 and 270, and cross flow velocities were 0.227 m/s and 0.136 m/s respectively. Each test was conducted for 30 minutes and samples were taken from permeate stream every 5 minutes, as well as measuring the flow rate. The flow rate was converted to flux, then to permeance and permeance versus time graph was plotted for each membrane. In addition to the permeance values, fouling resistances of the membranes were calculated using Darcy's Law:

$$J = \frac{TMP}{\mu \times R_{tot}}$$

Where J is the flux in L/m²h, TMP is the trans membrane pressure in bar, μ is the permeate viscosity and R_{tot} is the total flow resistance on the membrane in m⁻¹.

Using the total resistance, and the intrinsic resistance that was calculated during pure water permeance tests, fouling resistances of the membranes were calculated from the equation below:

$$R_f = R_{tot} - R_m$$

Where R_f is the fouling resistance, R_{tot} is the total resistance and R_m is the intrinsic membrane resistance to the flow in m⁻¹.

Finally, permeance during yeast filtration and pure water permeance of each membrane were compared by plotting permeance over pure water permeance versus time graph of the membrane.

CHAPTER 3

RESULTS AND DISCUSSION

3.1 Membrane Morphologies

Symmetric membranes are the membranes having a uniform pore size distribution throughout the cross section. Asymmetric membranes, on the other hand, are composed of a relatively dense skin layer with the addition of a support layer on it that has larger pore sizes. The asymmetry occurs during the induction of the non-solvent; the solvent is replaced by non-solvent via diffusion during liquid induced phase separation, and the membrane cast from the polymer solution starts to coagulate. Starting at the interface between the solvent and non-solvent, a skin layer forms during coagulation and slows down the diffusion; resulting in more time for nucleus growth within the membrane, and therefore larger pores after the skin layer^[46]. Membrane pore sizes and morphologies are determined by the time the solution spends between the binodal and spinodal boundaries of ternary phase diagram shown in Figure 3.1. Examples of symmetric and asymmetric membranes are shown in Figure 3.2:

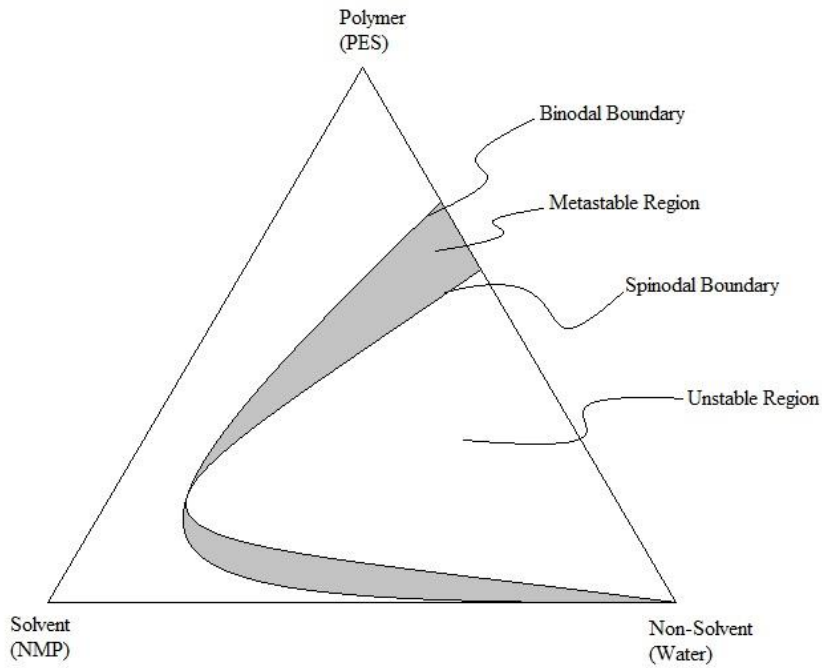


Figure 3.1: Ternary Phase Diagram of A Casting Solution

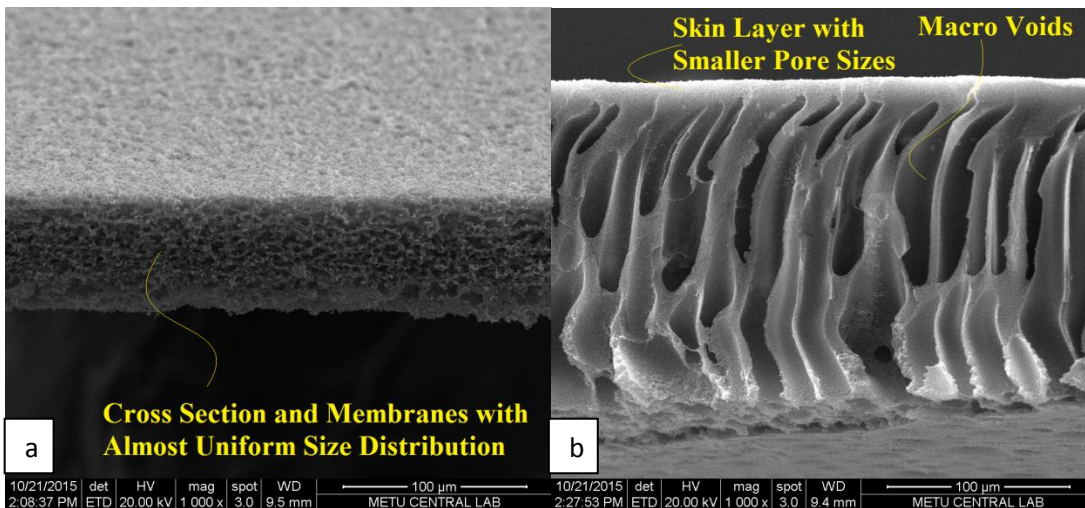


Figure 3.2: Membrane Examples a) Symmetric Flat PES Membrane (10% PES, exposed to humid air for 10 minutes) b) Asymmetric Flat PES Membrane (10% PES, exposed to humid air for 3 minutes) c) Symmetric Corrugated PES Membrane (10% PES, exposed to humid air for 5 minutes) d) Inverse Asymmetric Corrugated PES Membrane (10% PES, exposed to humid air for 4 minutes)

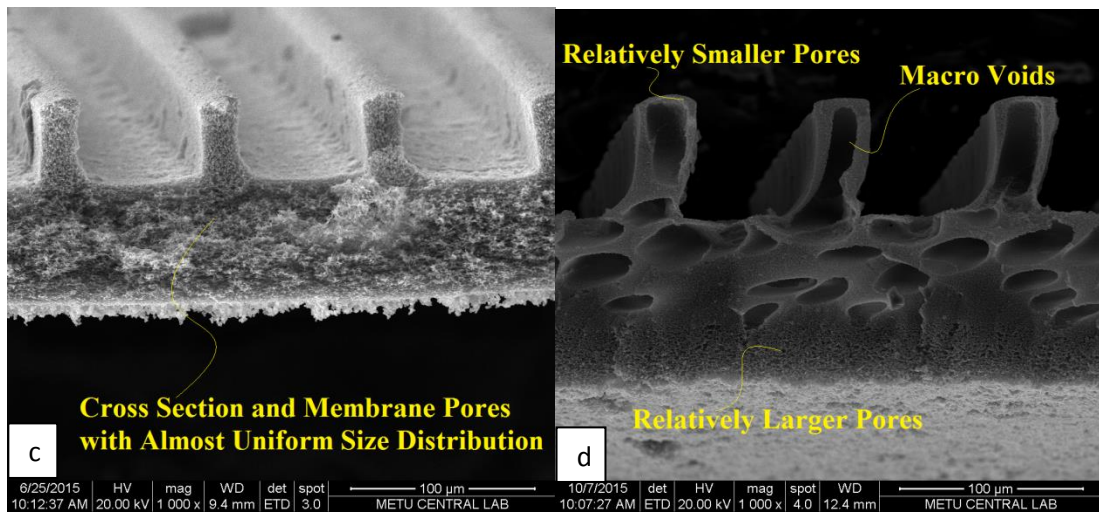


Figure 3.2 cont'd: Membrane Examples a) Symmetric Flat PES Membrane (10% PES, exposed to humid air for 10 minutes) b) Asymmetric Flat PES Membrane (10% PES, exposed to humid air for 4 minutes) c) Symmetric Corrugated PES Membrane (10% PES, exposed to humid air for 5 minutes) d) Inverse Asymmetric Corrugated PES Membrane (10% PES, exposed to humid air for 4 minutes)

The selective side of a membrane is skin layer, which makes it harder to produce corrugated membranes via phase separation micro fabrication since the skin layer is typically the layer that contacts with the non-solvent, and corrugations are formed on the mold side of a membrane via phase separation micro fabrication. Having a corrugated membrane with smaller pores on the mold side was achieved by Gençal et al. applying vapor induced phase separation for a certain period of time to a solution before coagulation, and resulting membrane will be an inverse asymmetric^[10] one with relatively smaller pores on the corrugated side and larger pores on the non-solvent side.

Since the aim was to produce patterned membranes via phase separation micro fabrication, the effects of vapor induced phase separation prior to coagulation were decided to be investigated deeply; humid air flow rate, humid air exposure time and relative humidity were altered to observe the effects, and to achieve the optimum morphology under the specified casting conditions.

3.1.1. Effect of Humid Air Flow Rate

The asymmetry occurs as a result of rapid replacement of solvent with non-solvent within the solution during liquid induced phase separation. The dense skin layer formed at the interface prevents the inner parts of the film to have the same diffusion rate and therefore results in an asymmetric pore size distribution. Vapor induced phase separation, on the other hand, does not cause an immediate exchange between the solvent and non-solvent and therefore it may lead to an almost uniform pore size distribution throughout the membrane cross section ^[46].

Corrugated membranes were exposed to humid air with flow rates of 0.9 L/min and 1.6 L/min, and the effects of different flow rates on the morphologies were observed via scanning electron microscopy images. Both membranes were exposed to humid air with relative humidity of 80% for 5 minutes prior to coagulation, and then coagulated in distilled water. Figure 3.3 shows the comparison of the effects of 0.9 L/min humid air exposure (on the left) with the effects of 1.6 L/min humid air exposure (on the right) on membrane morphologies:

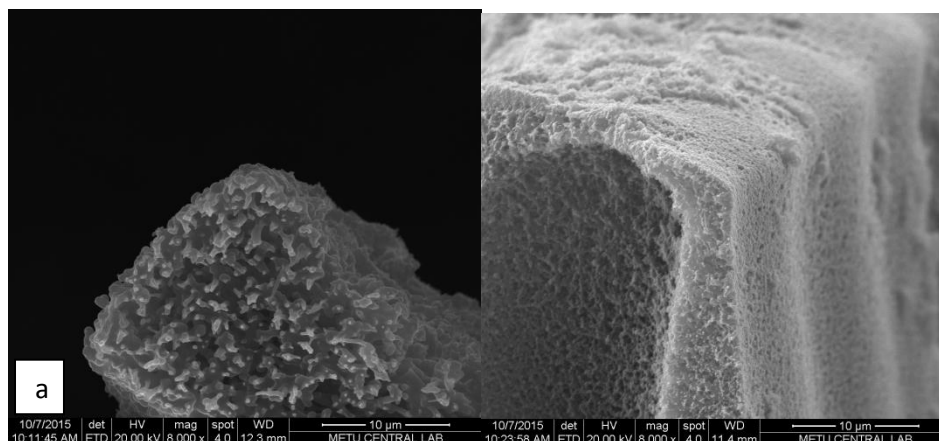


Figure 3.3: SEM Images of PES Membrane Exposed to 0.9 L/min Humid Air (on the left) and 1.6 L/min Humid Air (on the right) with a Relative Humidity of 80% for 5 minutes a) Corrugation Top b) Corrugation Bottom c) Non-Solvent Side d) Corrugated Surface e) Cross Section

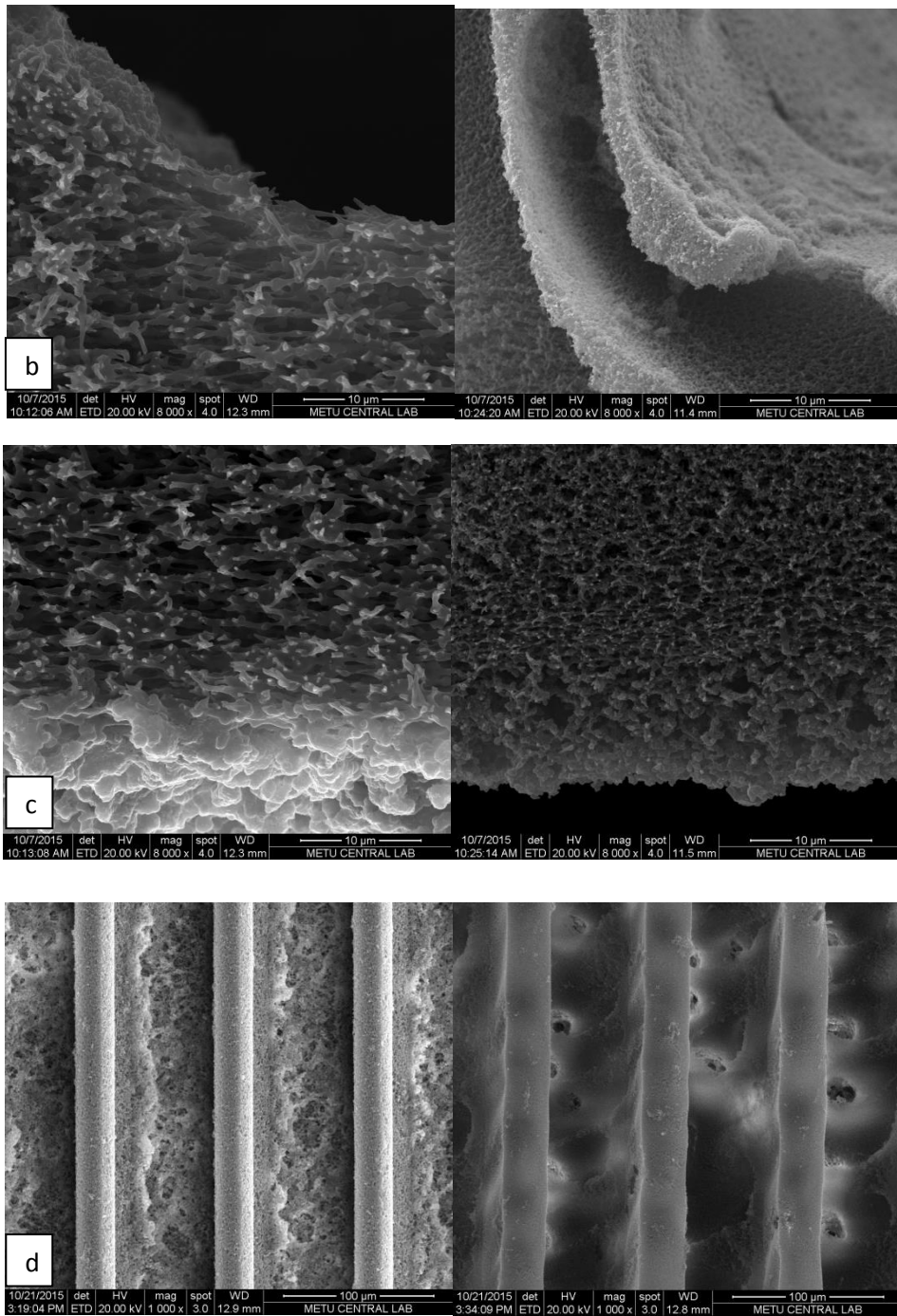


Figure 3.3 cont'd: SEM Images of PES Membrane Exposed to 0.9 L/min Humid Air (on the left) and 1.6 L/min Humid Air (on the right) with a Relative Humidity of 80% for 5 minutes a) Corrugation Top b) Corrugation Bottom c) Non-Solvent Side d) Corrugated Surface e) Cross Section

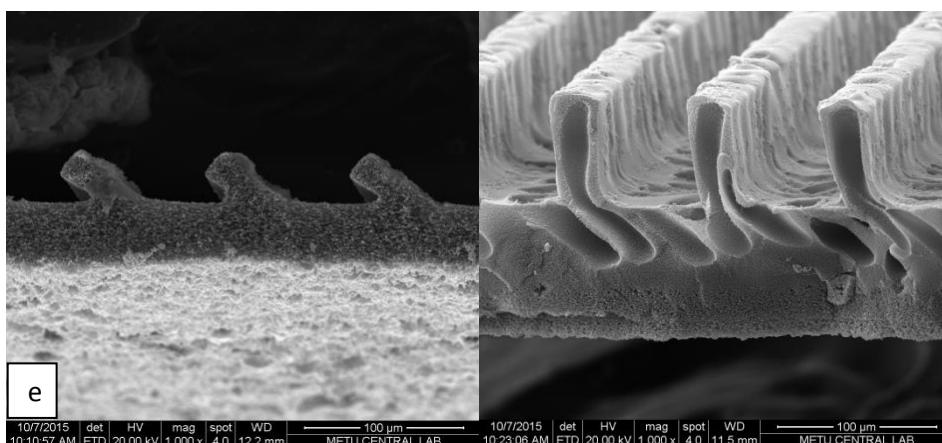


Figure 3.3 cont'd: SEM Images of PES Membrane Exposed to 0.9 L/min Humid Air (on the left) and 1.6 L/min Humid Air (on the right) with a Relative Humidity of 80% for 5 minutes a) Corrugation Top b) Corrugation Bottom c) Non-Solvent Side d) Corrugated Surface e) Cross Section

It can clearly be seen that increasing the humid air flow rate decreases the symmetry throughout the membrane cross section for 80% relative humidity. In addition to this, membrane pore sizes get slightly larger when the membrane is exposed to humid air with lower flow rate for the same duration. Table 3.1 shows the pore sizes of membranes exposed to different humid air flow rates:

Table 3.1: Pore Sizes of Membranes Exposed to Different Humid Air Flow Rates

| | Mold Side Pore Sizes (μm) | Non-Solvent Side Pore Sizes (μm) |
|--|--|---|
| 0.9 L/min Humid Air Exposure at 80% Relative Humidity for 5 minutes | 0.8-1.0 | 0.8-1.0 |
| 1.6 L/min Humid Air Exposure at 80% Relative Humidity for 5 minutes | 0.2-0.6 | 0.4-1.3 |

It was also observed that as they are exposed to higher humid air flow rates, the overall thickness of the membranes increases. Table 3.2 shows the change of these dimensions with the change in humid air flow rate:

Table 3.2: Dimensions of Corrugated Membranes Exposed to Humid Air at 80% Relative Humidity 0.9 L/min and 1.6 L/min for 5 minutes

| | a (μm) | b (μm) | c (μm) | d (μm) |
|---|---------------|---------------|--|----------------------|
| 0.9 L/min Humid Air Exposure for 5 minutes | 24±5 | 28±10 | 87±20 | 43±10 |
| | Fidelity=0.5 | Fidelity=0.4 | S _{N+} = 0.7 S _{N-} = 0.8 | S _L = 0.3 |
| 1.6 L/min Humid Air Exposure for 5 minutes | 35±5 | 65±5 | 143±10 | 52±10 |
| | Fidelity=0.7 | Fidelity=1 | S _{N+} = 0.5 S _{N-} = 0.7 | S _L = 0.1 |

Table 3.2 also shows that all the dimensions of membrane that is exposed to 0.9 L/min humid air flow rate are smaller, which can be attributed to the fact that there were no macro voids observed in the structures of membranes produced 0.9 L/min humid air flow rate. In addition, height and width fidelities increase with increasing humid air flow rate whereas both lateral and normal shrinkages decrease.

3.1.2. Effect of Humid Air Exposure Time

In order to further examine the effects of vapor induced phase separation prior to coagulation, membranes were exposed to humid air with relative humidity of 80%, at the flow rate of 0.9 L/min; the exposure times were altered as 5, 4 and 3 minutes. Figure 3.3 had shown the results of 5 minutes exposure, Figure 3.4 shows 4 minutes and Figure 3.5 shows 3 minutes exposure times:

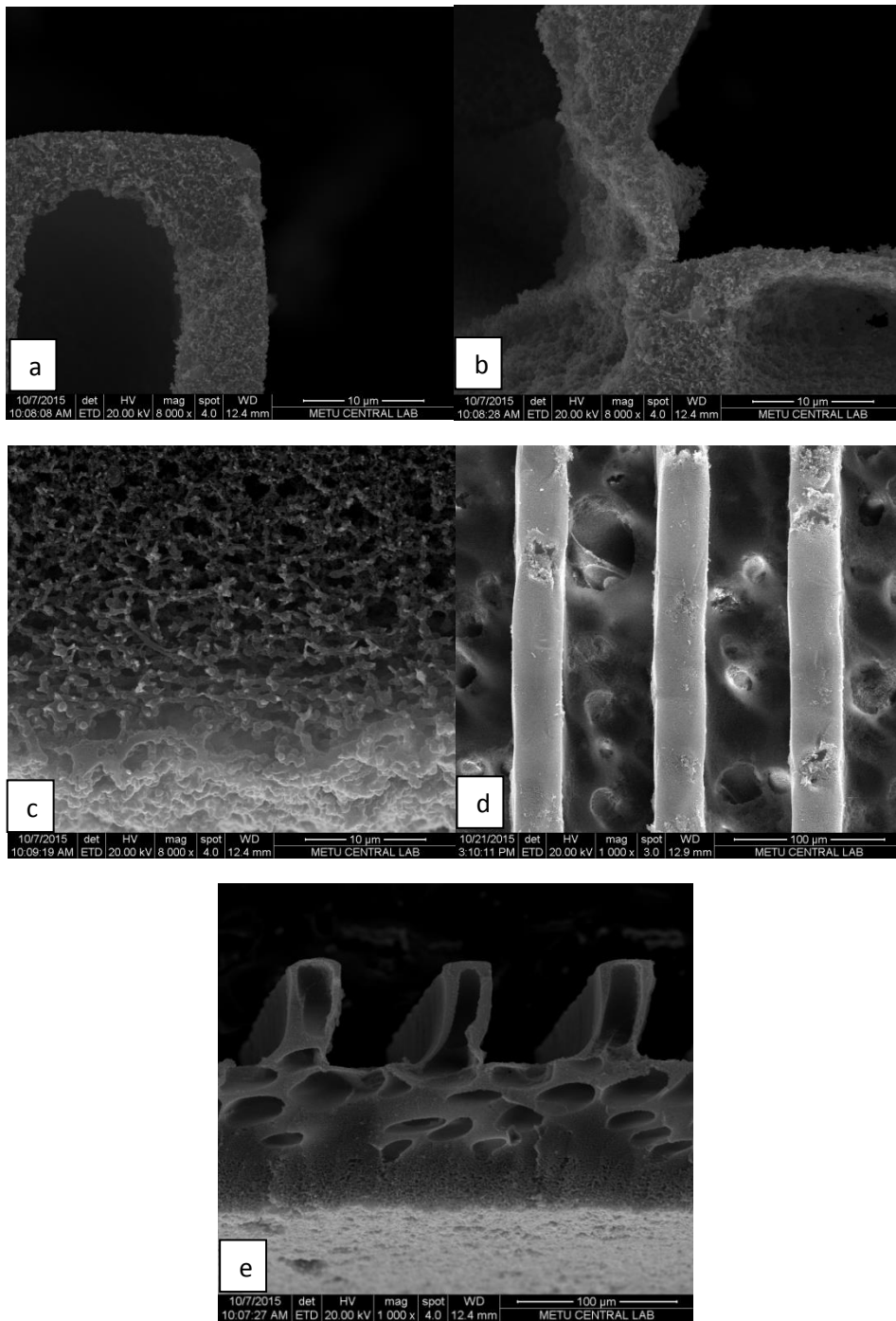


Figure 3.4: SEM Images of the Membrane Exposed to Humid Air for 4 Minutes, at 0.9 L/min Flow Rate with Relative Humidity of 80% a) Corrugation Top b) Corrugation Bottom c) Non-Solvent Side d) Corrugated Surface e) Cross Section

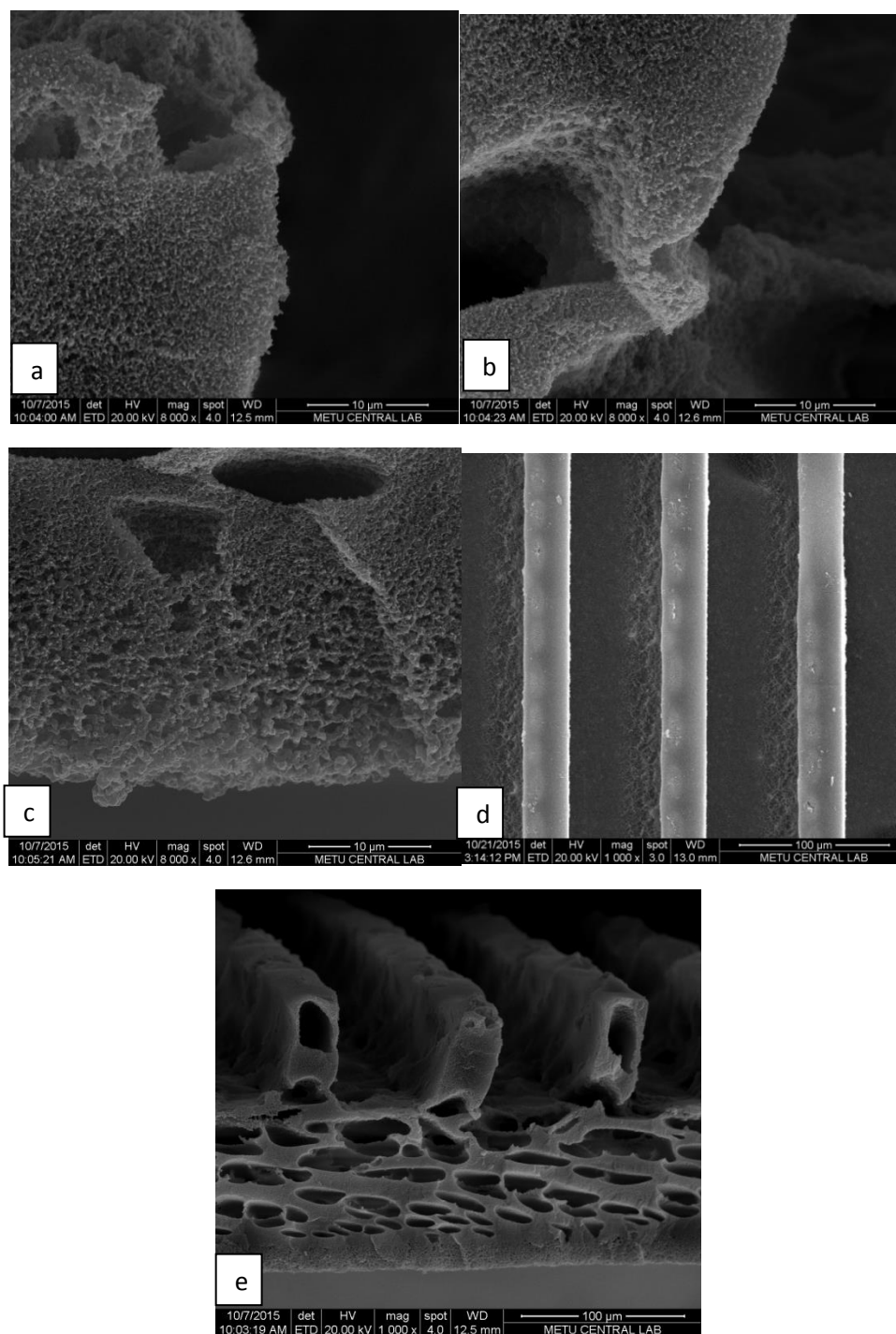


Figure 3.5: SEM Images of the Membrane Exposed to Humid Air for 3 Minutes, at 0.9 L/min Flow Rate with Relative Humidity of 80% a) Corrugation Top b) Corrugation Bottom c) Non-Solvent Side d) Corrugated Surface e) Cross Section

The figures show that under the conditions of 80% relative humidity and 0.9 L/min humid air flow rate, increasing humid air exposure time results in an increase of membrane symmetry. While 5 minutes exposed membranes have almost uniform pore size distribution throughout the cross section, this morphology is not observed at 4 and 3 minutes exposure times. Inverse asymmetry started to be seen at 4 minutes exposure time, and is also observed in 3 minutes exposure time. The pore sizes of membranes having 3 and 4 minutes exposure times are given below in Table 3.3:

Table 3.3: Pore Sizes of Membranes Having Different Exposure Times

| | Mold Side Pore Sizes (μm) | Non-Solvent Side Pore Sizes (μm) |
|--|--|---|
| 0.9 L/min Humid Air Exposure at 80% Relative Humidity for 5 minutes | 0.8-1.0 | 0.8-1.0 |
| 0.9 L/min Humid Air Exposure at 80% Relative Humidity for 4 minutes | 0.2-1.0 | 0.6-1.2 |
| 0.9 L/min Humid Air Exposure at 80% Relative Humidity for 3 minutes | 0.4-0.8 | 0.7-1.6 |

The change in the dimensions of corrugated membranes can be observed in Table 3.4, where the dimensions are given below:

Table 3.4: Dimensions of Corrugated Membranes Exposed to Humid Air at 80% Relative Humidity 0.9 L/min for 5, 4 and 3 minutes

| | a (μm) | b (μm) | c (μm) | d (μm) |
|---|----------------------|-----------------------|---|-------------------------------|
| 0.9 L/min Humid Air Exposure for 5 minutes | 24±5 Fidelity=0.5 | 28±10 Fidelity=0.4 | 87±20 S _{N+} = 0.7 S _{N-} = 0.8 | 43±10 S _L = 0.3 |
| 0.9 L/min Humid Air Exposure for 4 minutes | 35±5 Fidelity=0.7 | 65±10 Fidelity=1 | 152±5 S _{N+} = 0.5 S _{N-} = 0.7 | 61±10 S _L = 0 |
| 0.9 L/min Humid Air Exposure for 3 minutes | 30±2 Fidelity=0.6 | 65±2 Fidelity=1 | 165±2 S _{N+} = 0.5 S _{N-} = 0.6 | 70±2 S _L = 0 |

Pattern fidelities of the membranes seem to decrease while both lateral and normal shrinkages increase with increasing humid air exposure time. In addition, as the structure approaches to symmetry, shrinkage increases both in lateral and normal directions. Lateral shrinkage, however, is very low compared to normal shrinkage in all cases as reported by other colleagues ^[46, 48-49].

3.1.3. Effect of Relative Humidity

In order to observe how relative humidity affects the membrane morphology during vapor induced phase separation, the cast solution was exposed to humid air with relative humidity of 80% and 50% for 5 minutes. Figure 3.6 shows the comparison between the cross sections of these membranes:

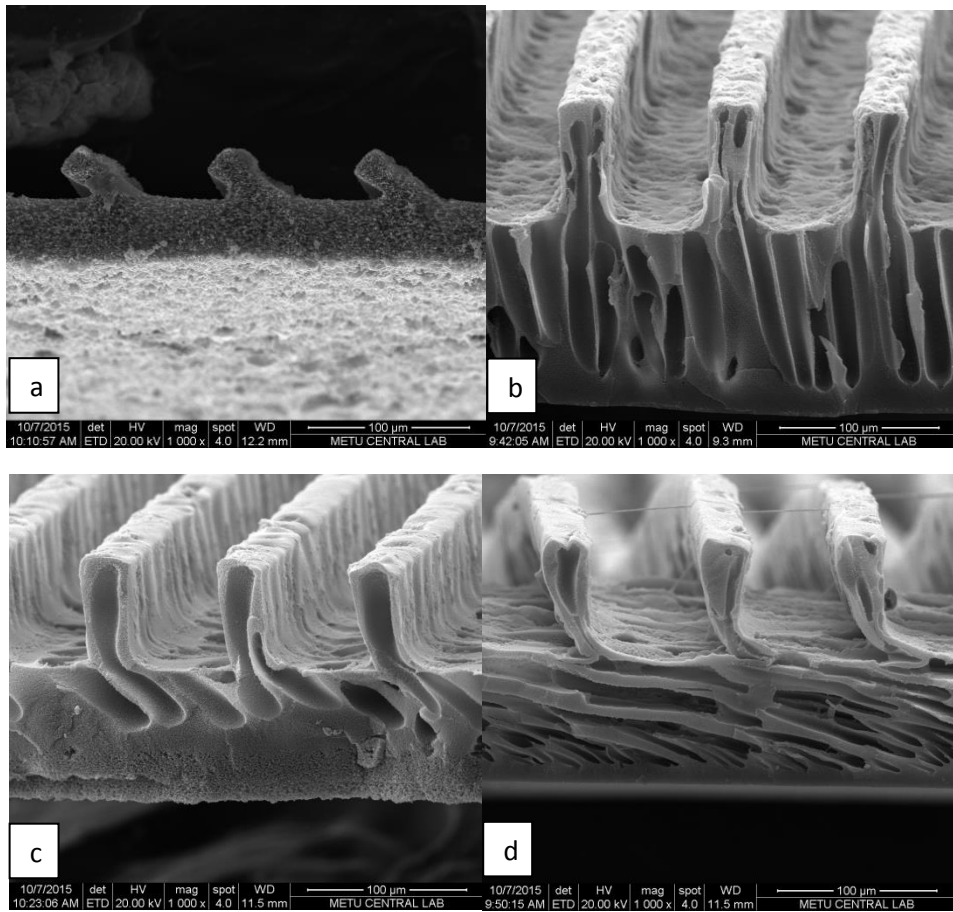


Figure 3.6: Cross Sections of Membranes Exposed to Different Relative Humidity for 5 Minutes a) 80% Relative Humidity with 0.9 L/min b) 50% Relative Humidity with 0.9 L/min c) 80% Relative Humidity with 1.6 L/min d) 50% Relative Humidity with 1.6 L/min

The results show that there is a dense skin layer on the non-solvent side, the side where there are no corrugations, at the membranes that are exposed to humid air with relative humidity of 50%. This means that, contrary to 80% relative humidity, these membranes have asymmetric structures rather than inverse asymmetric ones.

It can also be observed that morphology throughout the cross section is not significantly affected with the change of humid air flow rate for 50% relative humidity. In order to further investigate this effect, the cast solution was exposed to humid air of 50% relative humidity for 10 minutes as well. Figure 3.7 shows the SEM images of these membranes:

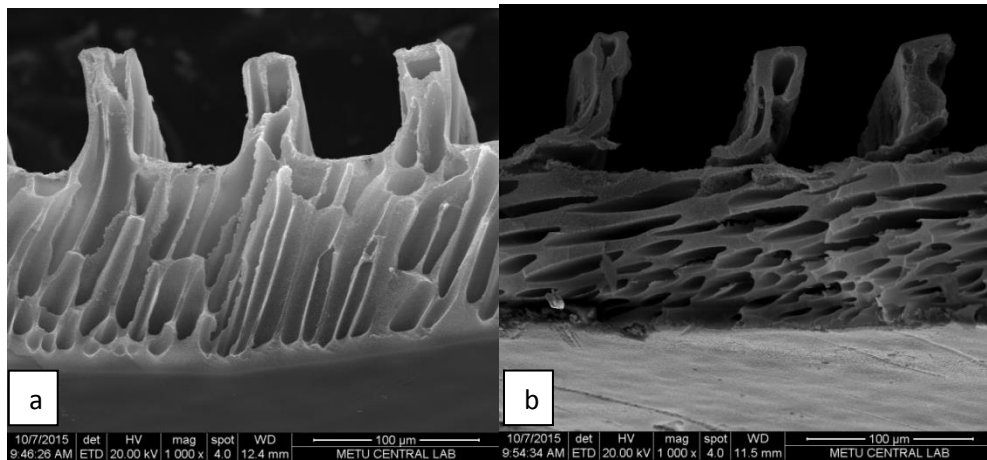


Figure 3.7: Cross Sectional SEM Images of Membranes Exposed to Humid Air with Relative Humidity of 50% for 10 minutes a) 0.9 L/min Humid Air Flow Rate b) 1.6 L/min Humid Air Flow Rate

The figures show that dense skin layer on the non-solvent side continues existing in the morphology for 10 minutes exposure time too, resulting in the asymmetry. Finally, Table 3.5 shows the effect of relative humidity on the dimensions of the corrugated membranes:

Table 3.5: Dimensions of Corrugated Membranes Exposed to Humid Air at 50% Relative Humidity

| | a (μm) | b (μm) | c (μm) | d (μm) |
|---|---------------|---------------|----------------------------------|---------------|
| 0.9 L/min Humid Air Exposure for 5 minutes | 26 | 70 | 187 | 65 |
| | Fidelity=0.5 | Fidelity=1.1 | $S_{N+} = 0.4$ $S_{N-} = 0.5$ | $S_L = 0.1$ |
| 1.6 L/min Humid Air Exposure for 5 minutes | 23 | 65 | 152 | 65 |
| | Fidelity=0.5 | Fidelity=1 | $S_{N+} = 0.5$ $S_{N-} = 0.7$ | $S_L = 0.1$ |

Table 3.5 cont'd: Dimensions of Corrugated Membranes Exposed to Humid Air at 50% Relative Humidity

| | | | | |
|--|--------------------|------------------|---|-----------------|
| 0.9 L/min Humid Air Exposure for 10 minutes | 35 Fidelity=0.7 | 65 Fidelity=1 | 196 $S_{N+} = 0.4$ $S_{N-} = 0.5$ | 65 $S_L = 0$ |
| 1.6 L/min Humid Air Exposure for 10 minutes | 30 Fidelity=0.6 | 65 Fidelity=1 | 161 $S_{N+} = 0.5$ $S_{N-} = 0.6$ | 70 $S_L = 0$ |

The dimensions were observed to get slightly larger with increasing humid air exposure time and decreasing humid air flow rate for 50% relative humidity. Shrinkage and fidelity do not seem to change significantly since phase separation takes place rapidly, as reported by other authors^[31]. Since the features of the patterns constrain the lateral shrinkage by holding the polymer replica in mold channels, it is harder to observe especially lateral shrinkage for these membranes. The small shrinkage observed, on the other hand, shows that shrinkage continues after humid exposure and during the washing step. Flat membranes were observed under SEM as well, in order to further investigate the parameters affecting the membrane morphologies. Table 3.6 shows the cross sectional SEM images of the flat membranes produced changing the same parameters as corrugated ones:

Table 3.6: Cross Sectional SEM Images of Flat Membranes

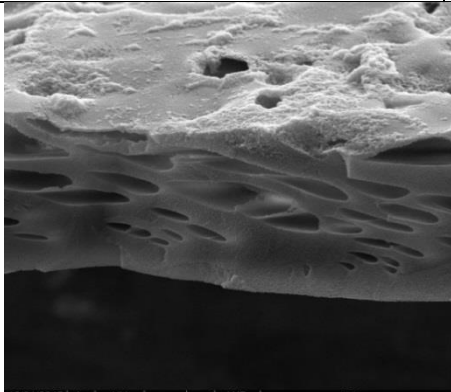
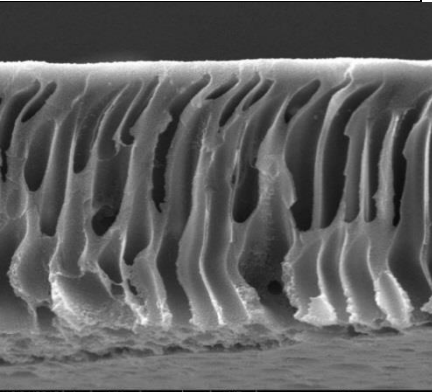
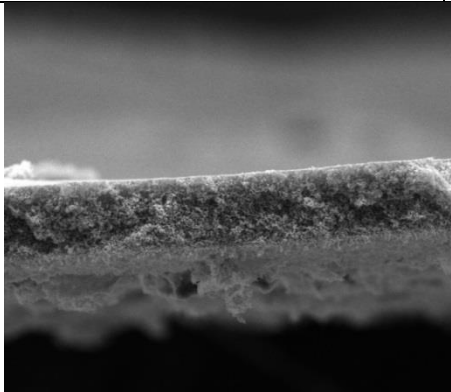
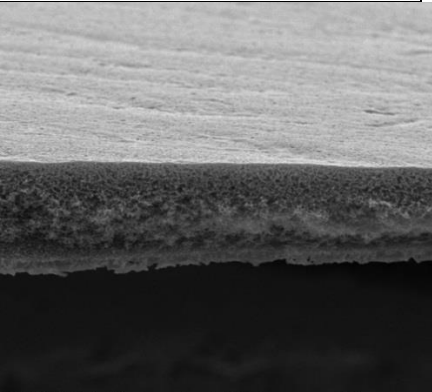
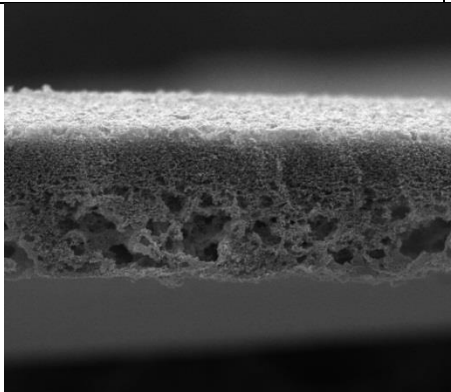
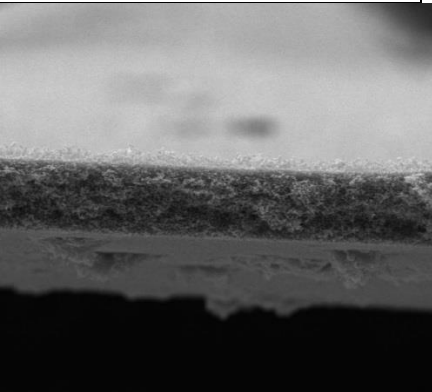
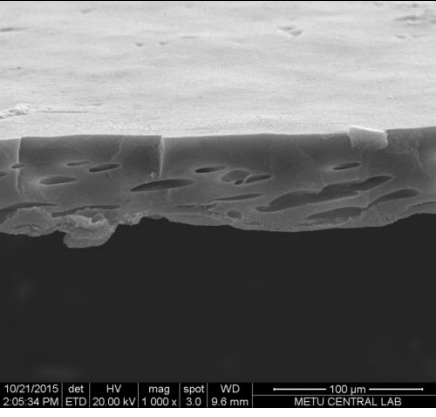
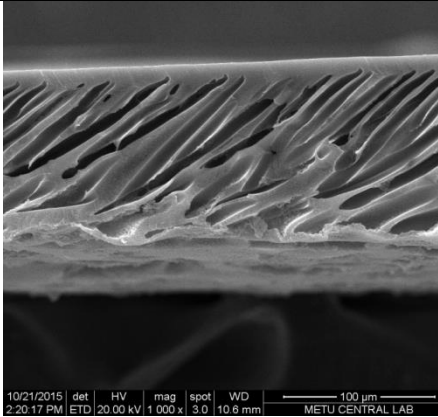
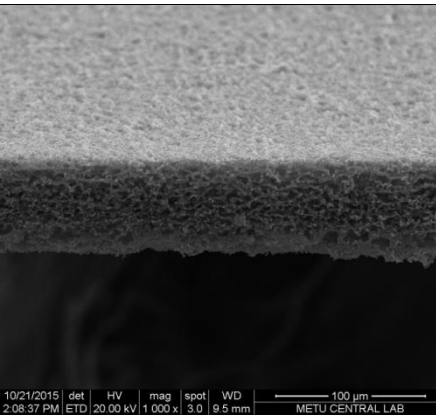
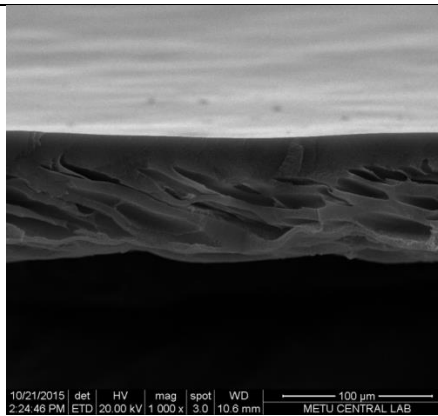
| | 0.9 L/min Humid Air Flow Rate | 1.6 L/min Humid Air Flow Rate |
|--|---|--|
| Relative Humidity: 80% Humid Air Exposure Time: 3 minutes |  |  |
| Relative Humidity: 80% Humid Air Exposure Time: 4 minutes |  |  |
| Relative Humidity: 80% Humid Air Exposure Time: 5 minutes |  |  |

Table 3.6 cont'd: Cross Sectional SEM Images of Flat Membranes

| | | |
|--|--|---|
| <p>Relative Humidity: 50%</p> <p>Humid Air Exposure Time: 5 minutes</p> |  |  |
| <p>Relative Humidity: 50%</p> <p>Humid Air Exposure Time: 10 minutes</p> |  |  |

The figures show, just as with the corrugated membranes, that symmetry increases with increasing humid air exposure time for all the membranes; this result can be attributed to the fact that increasing humid air exposure time results in more time for nuclei growth during phase inversion, which leads to an almost uniform pore size distribution as the humid air exposure time increases. It can also be inferred from the figures that increasing humid air flow rate results in a decrease in the symmetry for all the membranes; while the structure gets closer to symmetric after 4 minutes exposure for 0.9 L/min flow rate at 80% relative humidity, there is still a thin skin layer at the same exposure time for 1.6 L/min flow rate and the structure gets symmetric at 5 minutes exposure for both flow rates. It can be imputed to residence time the polymer solution spends in the humid air exposure box during vapor induced phase separation; increasing the time the solution spends before coagulation results in the structure to get closer to symmetric. For 50% relative humidity, on the

other hand, the skin layer can still be observed with macro voids for 0.9 L/min flow rate and with finger like structure for 1.6 L/min flow rate. The structure gets symmetric at 10 minutes exposure for 50% relative humidity and 0.9 L/min flow rate, while the finger like structure keeps on existing for 1.6 L/min humid air flow rate at 50% relative humidity. This result can be attributed to the fact that there is less vapor sorption for the same time spent at smaller relative humidity, which results in a smaller driving force for phase separation since the water vapor concentration is less in the humid air, and therefore on the polymer solution side of the interface, so it takes a longer residence time for the structure to go symmetric.

The thicknesses of these flat membranes were measured too for comparison, and results can be seen in Table 3.7:

Table 3.7: Thickness Values of Flat Membranes

| | 0.9 L/min Humid Air Flow Rate (μm) | 1.6 L/min Humid Air Flow Rate (μm) |
|---|---|---|
| Relative Humidity: 80% | 97 | 176 |
| Humid Air Exposure Time: 3 minutes | $S_N = 0.6$ | $S_N = 0.3$ |
| Relative Humidity: 80% | 48 | 54 |
| Humid Air Exposure Time: 4 minutes | $S_N = 0.8$ | $S_N = 0.8$ |
| Relative Humidity: 80% | 82 | 45 |
| Humid Air Exposure Time: 5 minutes | $S_N = 0.7$ | $S_N = 0.8$ |

Table 3.7 cont'd: Thickness Values of Flat Membranes

| | | |
|--|-------------|-------------|
| Relative Humidity: 50% | 66 | 117 |
| Humid Air Exposure Time: 5 minutes | $S_N = 0.7$ | $S_N = 0.5$ |
| Relative Humidity: 50% | 60 | 81 |
| Humid Air Exposure Time: 10 minutes | $S_N = 0.8$ | $S_N = 0.7$ |

The thickness measurements show us that increasing the humid air flow rate results in thicker membranes, which can be attributed to the fact that asymmetric membranes are thicker due to their structures with macro voids; symmetry results in membrane thickness to decrease since the pore sizes decrease because of the disappearance of macro voids. Similar to the behavior in corrugated membranes, shrinkage increases as the morphology gets closer to symmetric. The difference in the extent of shrinkage for flat and corrugated membranes can be attributed to a combination of the longer route the water vapor needs to take and mold constraining the shrinkage for corrugated membranes. Pore sizes of the flat membranes were also measured, which was shown in Table 3.8:

Table 3.8: Flat Membrane Pore Sizes

| | 0.9 L/min Humid Air Flow Rate (μm) | 1.6 L/min Humid Air Flow Rate (μm) |
|---|---|---|
| Relative Humidity: 80% | 0.3-0.5 | 0.2-0.4 |
| Humid Air Exposure Time: 3 minutes | | |

Table 3.8 cont'd: Flat Membrane Pore Sizes

| | | |
|---|---------|---------|
| <p>Relative Humidity: 80%</p> <p>Humid Air Exposure Time: 4 minutes</p> | 0.9-1.3 | 0.6-1.4 |
| <p>Relative Humidity: 80%</p> <p>Humid Air Exposure Time: 5 minutes</p> | 1.6-1.9 | 0.9-1.2 |
| <p>Relative Humidity: 50%</p> <p>Humid Air Exposure Time: 5 minutes</p> | 0.3-0.7 | 0.1-0.2 |
| <p>Relative Humidity: 50%</p> <p>Humid Air Exposure Time: 10 minutes</p> | 1.1-1.4 | 0.3-0.5 |

The comparison of pore sizes give us that increasing humid air exposure time, decreasing humid air flow rate and increasing relative humidity results in the pore sizes to increase for flat membranes, just as observed for corrugated membranes. In addition, when the corrugated and flat membranes produced under same conditions are compared, it can be seen that flat membranes have larger pore sizes throughout

the cross section and the difference between pore sizes increase with increasing exposure time. This can be a result of the extra depth introduced by corrugations on the mold; while the flat membranes have 250 μm thickness, corrugations add an extra 65 μm depth to the polymer volume used, and this results in water vapor to have a longer route to take during vapor induced phase separation. As a result, for the same exposure time when vapor induced phase separation is introduced before liquid induced phase separation, there will be more nuclei growth for the flat membranes due to having a thinner path. When there is no vapor induction prior to liquid induction, or when relative humidity is low during vapor induction, there would not be enough time for nuclei growth throughout the cross section and rapid exchange would result in a skin layer at the interface of solvent and non-solvent. Vapor induction, on the other hand, results in enough time for nuclei growth throughout the cross section and a more open structure; this structure may lead to a faster coagulation on the mold side during water immersion, and as a result a skin layer on the mold side. The fact that there is inverse asymmetry only in the corrugated membranes and there is rather asymmetry in the flat membranes can also be explained with this.

Altering the humid air flow rate, humid air exposure time and relative humidity has resulted in a variety of morphologies for corrugated membranes. Given that it was desired to have inverse asymmetric structures; the membranes were compared for their behavior in symmetry, their dimensions and structures. It was observed that all three variables had vital effects on membrane morphologies; the corrugated membrane exposed to relative humidity of 80%, with humid air flow rate of 0.9 L/min for 4 minutes was observed to have the most inverse asymmetric structure. Therefore these membranes were chosen to proceed with performance tests, and to be compared with their flat counterparts.

3.2. Performance Tests

3.2.1. Pure Water Permeances

Before starting fouling tests, membranes were tested for their pure water permeances in order to determine the effect of polydopamine coating on the pure water

permeances of both flat and corrugated membranes. For this purpose, the membranes were coated with polydopamine for 24 hours as defined in experimental methods part. In the beginning, it was determined to coat the membranes for one hour and shake vertically in addition to being coated after being dried, and therefore being treated with oxygen plasma to increase the effectiveness of coating. However, when one hour coating did not turn out to be effective, it was determined to coat the membranes for 24 hours and shaking was determined to be rotationally. In addition, membranes were started to be coated without drying and oxygen plasma. Figure 3.8 shows the results of pure water permeance tests:

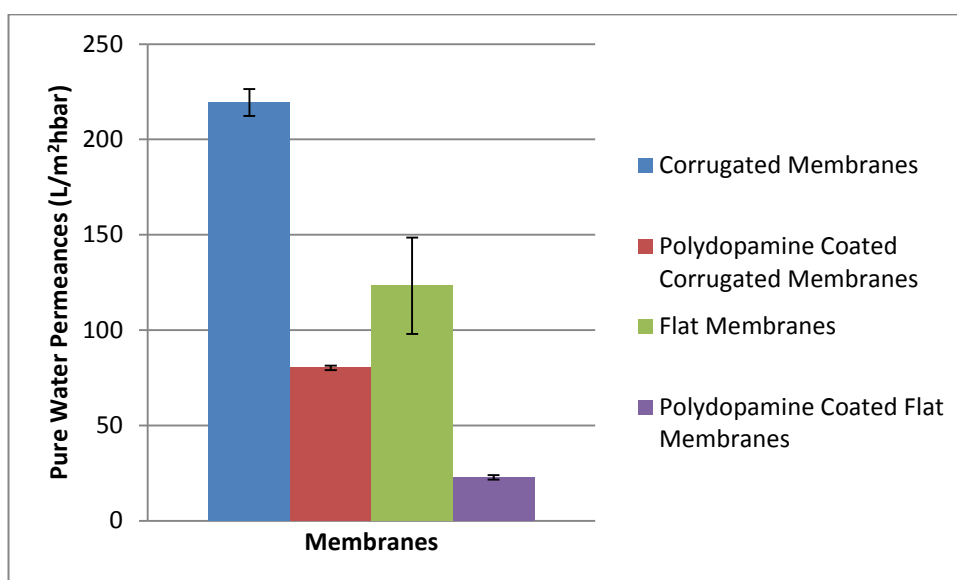


Figure 3.8: Pure Water Permeance Values of the Membranes

First result that can be inferred from the figure is that there is nearly a 100% difference between the pure water permeance values of flat and corrugated membranes. These calculations are done with normalized surface area for corrugated membranes, which have actual areas that are twice the flat ones do, due to the corrugations on the surface. Therefore, this 100% difference between the flat and corrugated membranes can be explained with the surface area difference, given that there is no significant difference between the pore sizes of flat and corrugated membranes.

Secondly, it can be seen that polydopamine coating has decreased the pure water permeance of flat and corrugated membranes as expected; this decrease can be roughly estimated as threefold for corrugated membranes, and sixfold for flat ones. By observing the pure water permeance results, it can be said that polydopamine coating has slightly decreased the pore sizes of the membranes. In order to further investigate the polydopamine coating, FTIR and EDX analyses were conducted on the coated membranes. Figure 3.9 shows the FTIR results:

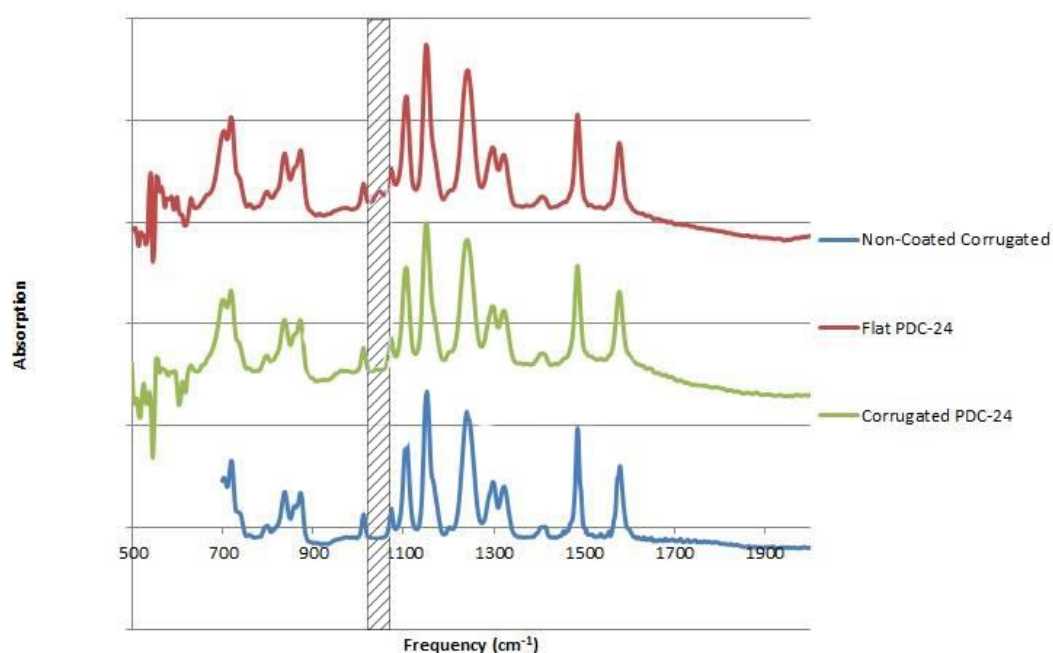


Figure 3.9: FTIR Results of the Membranes

The small peak around 1045 cm⁻¹ on both flat and corrugated polydopamine coated membranes indicate C-N stretch for amines^[47], and therefore can be taken as a sign of polydopamine on the surface. Table 3.9 shows the EDX results on the surface of the coated membranes:

Table 3.9: Elemental Weight Percentages taken from EDX Results of Polydopamine Coated Membranes

| | Uncoated Corrugated Membrane | Uncoated Flat Membrane | Coated Flat Membrane | Coated Corrugated Membrane |
|-----------------|---|---------------------------------------|---------------------------------|---|
| Carbon | 63.87 | 71.94 | 78.51 | 75.53 |
| Nitrogen | - | - | 1.52 | 2.06 |
| Oxygen | 9.06 | 13.02 | 9.98 | 10.70 |
| Sulfur | 27.07 | 15.04 | 9.99 | 11.71 |

The EDX results taken from both on the corrugations and between the corrugations show traces of nitrogen on the surfaces of both flat and corrugated membranes, which is not present in polyethersulfone. The fact that the nitrogen amount is very low can be explained by the polydopamine layer being in the scale of nanometers; therefore it can be inferred from the EDX results that the polydopamine coating has been successful on the membrane surfaces. The coating can be observed on the surface photographs of the membranes when coated and uncoated membranes were compared, Figure 3.10 shows this comparison:

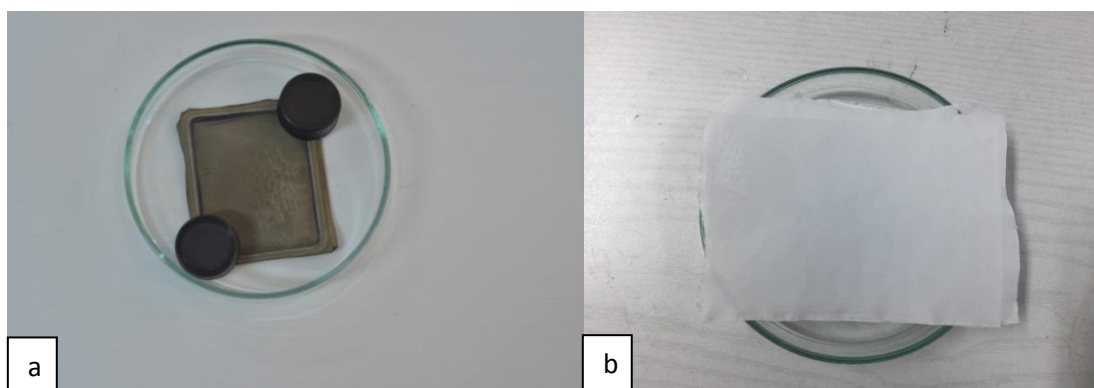


Figure 3.10: Surfaces of Coated and Uncoated Corrugated membranes a) Coated Corrugated Membrane b) Uncoated Corrugated Membrane

Finally, SEM images of coated and non-coated membranes were taken to see the effects of polydopamine coating on the surface morphology. Figure 3.11 shows the SEM images of these membranes:

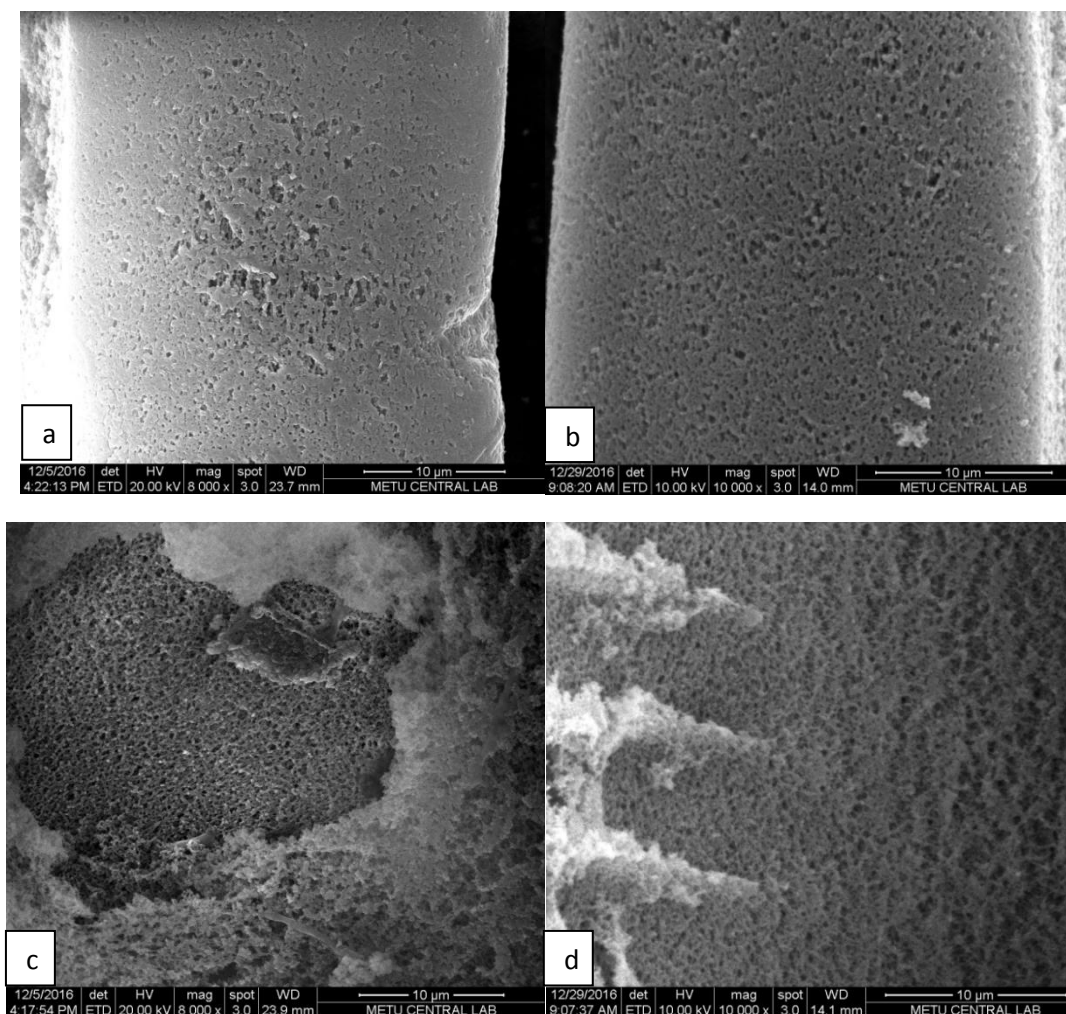


Figure 3.11: Closer Look Up on Surfaces of Coated and Non-Coated Membranes a) On Corrugation of Polydopamine Coated Membrane b) On Corrugation of Non-Coated Membrane c) Between the Corrugations of Polydopamine Coated Membrane d) Between the Corrugations of Non-Coated Membrane

In order to observe whether there is pore size reduction in the polydopamine coated corrugated membranes, BSA rejection (66 kDa) was measured. The permeance and rejection of the membranes were calculated during the filtration, as explained in the

experimental methods. It was found out that there is nearly no rejection of BSA, meaning that despite being able to decrease the pure water permeance, polydopamine coating was not able to reduce the pore size enough for BSA rejection. Figure 3.15 also reveals that there are layers of polydopamine on the membrane surfaces, however the coating does not seem to be homogenous and therefore this might be the reason for observing pure water permeance to decrease but no rejection for BSA.

3.2.2. Fouling Performances

Performance observations were continued with yeast fouling tests, where 0.025 weight percent yeast was dispersed in ultrapure water and stirred at 250 rpm during filtration, yeast dispersion was permeated through the membranes with a Reynolds Number of 444, and fouling resistances as well as permeance during filtration over pure water permeance values were calculated as described in the experimental methods section. Figure 3.12 shows the comparison of fouling resistances of uncoated and coated flat and corrugated membranes, where flat membranes are indicated by orange and corrugated membranes are indicated by blue colors, and where the lines of the same colors indicate the repeat experiments for the same conditions:

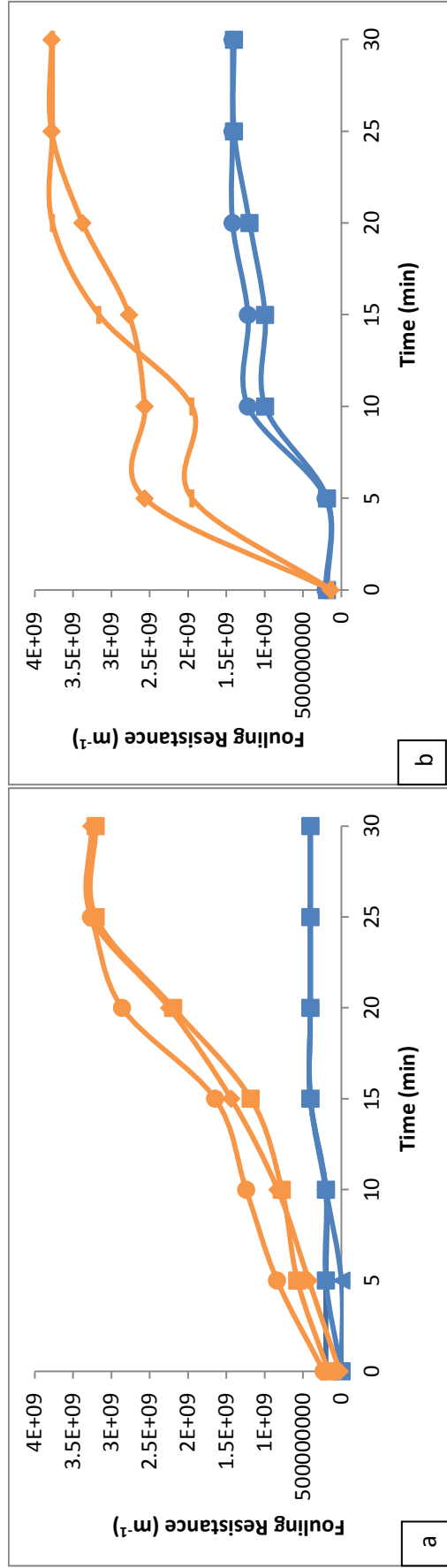


Figure 3.12: Comparison of the Fouling Resistances of Coated Flat and Corrugated Membranes for $Re=444$, Orange Indicates Flat Membranes while Blue Indicates Corrugated and Same Color Lines Indicate Repeat Experiments a) Uncoated Membranes b) Coated Membranes

Figures clearly show the difference of flow resistances caused by fouling between flat and corrugated membranes. While the fouling resistance increases slowly and stays constant after fifteen minutes for corrugated membranes, the increase continues until the end of the experiment for flat ones. The experiments were also conducted on polydopamine coated flat and corrugated membranes. The results again show a difference between the flow resistances caused by fouling when coated flat and coated corrugated membranes are compared with each other; there is almost four times difference between the fouling resistances, and coated corrugated membranes show better performance during yeast filtration. When coated and uncoated membranes are compared, on the other hand, polydopamine coating seems to have caused an increase in fouling for both types of membranes. While the performances of coated and uncoated flat membranes are closer to each other, there is a considerable difference between coated and uncoated corrugated membranes. This can be due to the coating being not homogenous on the membrane surface; while it may have been more successful on the corrugations, this result may have led to more fouling between the corrugations, where it seems less successful and where the membrane is more prone to fouling. In the case of smaller pores on the corrugations and larger pores between the corrugations, there might be more deposition between the corrugations, which can lead to a worse fouling behavior after coating. Since it gets harder to have a continuous coating with increasing surface roughness, the difference between coated and uncoated corrugated membranes is clearer. The difference between coated and uncoated membranes can also be as a result of a combination of the adhesive nature of yeast and weakly bound polydopamine present on the coated surface.

The fouling tests have shown that corrugated membranes demonstrate a better performance when compared to flat membranes, which was an expected result due to increasing the effective area and corrugations affecting the flow. In addition, despite resulting in small changes on performances of the membranes, polydopamine coating does not significantly improve the fouling behavior of neither the corrugated membranes, nor the flat ones. In fact, it negatively affected the fouling behavior of both flat and corrugated membranes. This effect is attributed to the fact that the

coating is not homogenous and it is discontinuous through the membrane surface, which resulted in pure water permeances to decrease but flow resistance caused by fouling to increase.

CHAPTER 4

CONCLUSIONS

Corrugated and flat membranes from PES were produced via phase separation micro molding in this study; their morphologies were tried to be tuned, examined under SEM and they were characterized with pure water permeance and yeast fouling tests. Conclusions below are reached at the end of the study:

1. With the recipe of 10% PES, 60% PEG-400, 25%NMP and 5% water; the closest structure to the desired inverse asymmetry for a corrugated membrane is the membrane exposed to humid air at 0.9 L/min flow rate, 80% relative humidity and for 4 minutes. In addition, their flat counterparts give an asymmetric membrane with a thin skin layer.
2. Symmetry behavior throughout the cross section decreases while overall membrane thickness and membrane pore sizes as well as pore sizes below the skin layer for asymmetric membranes, increase with increasing humid air flow rate during vapor induced phase separation. Symmetry behavior increases while pattern fidelity decreases with increasing humid air exposure time for 80% relative humidity, and inverse asymmetry is observed at 3 and 4 minutes exposure while morphology gets symmetric after 5 minutes for corrugated membranes. Membrane dimensions were observed to get larger with increasing humid air flow rate for 50% relative humidity. It was also observed that membranes produced in 50% relative humidity have asymmetric structures rather than inverse asymmetry, and this behavior does not

seem to change with increasing exposure time. Flat membranes were observed to have similar behavior under similar conditions, however inverse asymmetry was never observed in flat membranes.

3. Corrugated membranes were observed to have higher pure water permeance values, which was attributed to the 100% area enhancement as a result of introduced patterns, when compared to their flat counterparts. In addition, polydopamine coating has resulted in a decrease on pure water permeances of both type of membranes, however it did not result in any rejection for BSA solutions.

4. Fouling during yeast filtration was larger for both coated and uncoated flat membranes when they were compared with their corrugated counterparts. This, as expected, was attributed to the effects of corrugations on the surface. Polydopamine coating, on the other hand, have resulted in more fouling on the membranes. It resulted in the fouling behavior to increase, contrary to the expectations of increasing hydrophilicity and therefore fouling behavior. This can be resulted from the discontinuity of coating; the SEM images show that the polydopamine coating is not perfect and continuous, therefore this discontinuity may have resulted in worse fouling performance for the coated membranes.

5. As a suggestion; this study can be further conducted by changing the humid air flow rate, humid air exposure time and relative humidity during production more. It is also possible to alter the polydopamine coating process by changing the dopamine concentration or coating time. Membrane characterizations can be investigated more by working at higher Reynolds Numbers.

REFERENCES

- [1] Baker, R. (2012). *Membrane technology and applications* (3rd ed.). Chichester: J. Wiley
- [2] Mulder, M. (1991). *Basic Principles of Membrane Technology* (2nd ed.). Dordrecht: Kluwer Academic Publishers
- [3] Bikel, M., Pünt, I. G. M., Lammertink, R. G. H., Wessling, M. (2009). Micro-patterned polymer films by vapor-induced phase separation using permeable molds. *ACS Applied Materials & Interfaces*, 1(12), 2856-61.
- [4] Strahtmann, H., Scheible, P., Baker, R.W. (1971). A rationale for the preparation of Loeb-Sourirajan-type cellulose acetate membranes. *Journal of Applied Polymer Science*, 15(4), 811-828.
- [5] Strahtmann, H. (2011). *Introduction to Membrane Science and Technology* (1st ed.). Weinheim, Germany: Wiley-VCH Verlag & Co
- [6] Vogelaar, L., Lammertink, R. G. H., Barsema, J. N., Nijdam, W., Bolhuis-Wersteeg, L. A. M., van Rijn, C. J. M., Wessling, M. (2005). Phase separation micromolding: A new generic approach for microstructuring various materials. *Small*, 1(6), 645-655.
- [7] Matsuyama, H., Teramoto, M., Nakatani, R., Maki, T. (1999). Membrane formation via phase separation induced via penetration of nonsolvent from vapor phase. I . Phase diagram and mass transfer process. *Journal of Applied Polymer Science*, 74(1), 159-170.

- [8] Park, H. C., Hong, J. M., Ha, S. Y., Kang, Y. S., Ahn, K. S. (1998). Effects of humidity on the morphology of microporous membranes. *Journal of Industrial and Engineering Chemistry*, 4(1), 31-38.
- [9] van der Waal, M. J., Racz, I. G. (1989). Mass transfer in corrugated-plate membrane modules. I. Hyperfiltration experiments. *Journal of Membrane Science*, 40(2), 243-260.
- [10] Gençal, Y., Durmaz, E. N., Çulfaz-Emecen, P. Z. (2014). Preparation of patterned microfiltration membranes and their performance in crossflow yeast filtration. *Journal of Membrane Science*, 476 (2015), 224-233.
- [11] Scott, K., Mahmood, A., Jachuck, R., Hu, B. (2000). Intensified membrane filtration with corrugated membranes. *Journal of Membrane Science*, 173(1), 1-16.
- [12] Al-Malack, M. H., Anderson, G. K. (1996). Coagulation-crossflow microfiltration of domestic wastewater. *Journal of Membrane Science*, 121, 59-65.
- [13] Abdessemed, D., Nezzal, G., Ben Aim, R. (2000). Coagulation-adsorption-ultrafiltration for wastewater treatment and use. *Desalination*, 131, 307-314.
- [14] Howe, K. J., Marwah, A., Chiu, K. -P., Adham, S. S. (2006). Effect of coagulation on the size of MF and UF membrane foulants. *Environ. Sci. Technol.* 40, 7908-7913.
- [15] Reddy, A. V. R., Mohan, D. J., Bhattacharya, A., Shah, V. J., Ghosh, P. K. J. (2003). Surface modification of ultrafiltration membranes by preadsorption of a negatively charged polymer I. Permeation of water soluble polymers and inorganic salt solutions and fouling resistance properties. *Journal of Membrane Science*, 214(2), 211-221.
- [16] Ma, X., Su, Y., Sun, Q., Wan, Y., Jiang, Z. J. (2007). Enhancing the antifouling property of polyethersulfone membranes through surface adsorption-crosslinking of poly(vinyl alcohol). *Journal of Membrane Science*, 300(1-2), 71-78.

- [17] Galjaard, G., Buijs, P., Beerendonk, E., Schoonenberg, F., Schippers, J. C. (2001). Pre coating (EPCE (R)) UF membranes for direct treatment of surface water. *Desalination*, 139(1-3), 305-316.
- [18] Mu, L. -J., Zhao, W. -Z., (2009). Hydrophilic modification of polyethersulfone porous membranes via a thermal-induced surface crosslinking approach. *Applied Surface Science*, 255(16), 7273-7278.
- [19] King, S., Escobar, I., Xu, X. (2004). Ion Beam Irradiation Treatments of a Commercial Polyethersulfone Water-Treatment Membrane. *Environmental Chemistry*, 1(1), 55-59.
- [20] Kull, K. R., Steen, M. L., Fisher, E. R. J. (2005). Surface modification with nitrogen-containing plasmas to produce hydrophilic, low-fouling membranes. *Journal of Membrane Science*, 246(2), 203-215.
- [21] Wavhal, D. S., Fisher, E. R. J. (2002). Hydrophilic modification of polyethersulfone by low temperature plasma-induced graft polymerization. *Journal of Membrane Science*, 209(1), 255-269.
- [22] Wang, Y., Su, Y., Sun, Q., Ma, X., Jiang, Z. (2006). Generation of anti-biofouling ultrafiltration membrane surface by blending novel branched amphiphilic polymers with polyethersulfone. *Journal of Membrane Science*, 286(1-2), 228-236.
- [23] Rahimpour, A., Madaeni, S. S., Mehdipour-Ataei, S. J. (2008). Synthesis of a novel poly(amide-imide) (PAI) and preparation and characterization of PAI blended polyethersulfone (PES) membranes. *Journal of Membrane Science*, 311(1-2), 349-359.
- [24] Won, Y. -J., Lee, J., Choi, D. -C., Chae, H., Kim, I., Lee, C. -H., Kim, L. -C. (2012). Preparation and application of patterned membranes for wastewater treatment. *Environmental Science Technology*, 46(20), 11021-11027.
- [25] Zhang, L. -Z. (2005). Convective mass transport in cross-corrugated membrane exchangers. *Journal of Membrane Science*, 260, 75-83.

- [26] Hu, B., Scott, K. (2007). Influence of membrane material and corrugation and process conditions on emulsion microfiltration. *Journal of Membrane Science*, 294, 30-39.
- [27] Maruf, S. H., Wang, L., Greenberg, A. R., Pellegrino, J., Ding, Y. (2013). Use of nanoimprinted surface patterns to mitigate colloidal deposition on ultrafiltration membranes. *Journal of Membrane Science*, 428, 598-607.
- [28] Elimelech, M., Xiaohua, Z., Childress, A. E., Seungkwan, H. (1997). Role of membrane surface morphology in colloidal fouling of cellulose acetate and composite aromatic polyamide reverse osmosis membranes. *Journal of Membrane Science*, 127, 101-109.
- [29] Jamshidi Gohari, R., Lau, W. J., Matsuura, T., Ismail, A. F. (2013). Effect of surface pattern formation on membrane fouling and its control in phase inversion process. *Journal of Membrane Science*, 446, 326-331.
- [30] Lee, Y. K., Won, Y. -J., Yoo, J. H., Ahn, K. H., Lee, C. -H. (2013). Flow analysis and fouling on the patterned membrane surface. *Journal of Membrane Science*, 427, 320-325.
- [31] Won, Y. -J., Choi, D. -C., Jang, J. H., Lee, J. -W., Chae, H. R., Kim, I., Ahn, K. H., Lee, C. -H., Kim, I. -C. (2014). Factors affecting pattern fidelity and performance of a patterned membrane. *Journal of Membrane Science*, 462, 1-8.
- [32] Maruf, S. H., Greenberg, A. R., Ding, Y. (2016). Influence of substrate processing and interfacial polymerization conditions on the surface topography and permselective properties of surface-patterned thin-film composite membranes. *Journal of Membrane Science*, 512, 50-60.
- [33] ElSherbiny, I. M. A., Khalil, A. S. G., Ulbricht, M. (2017). Surface micro-patterning as a promising platform towards novel polyamide thin-film composite membranes of superior performance. *Journal of Membrane Science*, 529, 11-22.

- [34] Miller, D. J., Dreyer, D. R., Bielawski, C. W., Paul, D. R., Freeman, B. D. (2017). Surface modification of water purification membranes. *Angewandte Chemie International Edition*, 56, 4662-4711.
- [35] Elimelech, M., Phillip, W. A. (2011). The future of seawater desalination: Energy, technology and the environment. *Science*, 333, 712-717.
- [36] Fan, J., Luo, J., Chen, X., Wan, Y. (2016). Polydopamine meets porous membrane: A versatile platform for facile preparation of membrane adsorbers. *Journal of Chromatography*, 1448, 121-126.
- [37] Lee, H., Dellatore, S.M., Miller, W.M., Messersmith, P. B. (2007). Mussel-Inspired surface chemistry for multifunctional coatings. *Science*, 318, 426-430.
- [38] Lee, B. P., Messersmith, P. B., Israelachvili, J. N., Waite, J. H. (2011). Mussel-inspired adhesives and coatings. *Annu. Rev. Mater. Res.*, 41, 99-132.
- [39] McCloskey, B. D., Park, H. B., Ju, H., Rowe, B. W., Miller, D. J., Chun, B. J., Kin, K., Freeman, B. D. (2010). Influence of polydopamine deposition conditions on pure water flux and foulant adhesion resistance of reverse osmosis, ultrafiltration and microfiltration membranes. *Polymer*, 51, 3472-3485.
- [40] Jiang, J. -H., Zhu, L. -P., Li, X. -L., Xu, Y. -Y., Zhu, B. -K. (2010). Surface modification of PE porous membranes based on the strong adhesion of polydopamine and covalent immobilization of heparin. *Journal of Membrane Science*, 364, 194-202.
- [41] Cheng, C., Li, S., Zhao, W., Wei, Q., Nie, S., Sun, S., Zhao, C. (2012). The hydrodynamic permeability and surface property of polyethersulfone ultrafiltration membranes with mussel-inspired polydopamine coatings. *Journal of Membrane Science*, 417-418, 228-236.
- [42] Li, F., Meng, J., Ye, J., Yang, B., Tian, Q., Deng, C. (2014). Surface modification of PES ultrafiltration membrane by polydopamine coating and poly (ethylene glycol) grafting: Morphology, stability and anti-fouling. *Desalination*, 344, 422-430.

- [43] Yang, H. -C., Liao, K. -J., Huang, H., Wu, Q. -Y., Wan, L. -S., Xu, Z. -K. (2014). Mussel-inspired modification of a polymer membrane for ultra-high water permeability and oil-in-water emulsion separation. *Journal of Material Chemistry A*, 2, 10225-10230.
- [44] Miller, D. J., Kasemset, S., Wang, L., Paul, D. R., Freeman, B. D. (2014). Constant flux crossflow filtration evaluation of surface-modified fouling-resistant membranes. *Journal of Membrane Science*, 452, 171-183.
- [45] Madou, M. J. (2001). *Fundamentals of Microfabrication: The Science of Miniaturization* (2nd ed.). CRC Press.
- [46] Park, C. H., Kim, P., Kim, Y., Soo Kang, Y. (1999). Membrane formation by water vapor induced phase inversion. *Journal of Membrane Science*, 156 (2), 169-178.
- [47] Beauchamp. (n.d.). Infrared Tables (short summary of common absorption frequency) [pdf]. Retrieved from http://www.cpp.edu/~psbeauchamp/pdf/spec_ir_nmr_spectra_tables.pdf
- [48] Bikel, M., Pünt, I., Lammertink, R., Wessling, M. (2010). Shrinkage effects during polymer phase separation on microfabricated molds. *Journal of Membrane Science*, 347 (1-2), 141-149.
- [49] Aerts, P., Genné, I., Leysen, R., Jacobs, P., Vankelecom, I. (2006). The role of the nature of the casting substrate on the properties of membranes prepared via immersion precipitation. *Journal of Membrane Science*, 283 (1-2), 320-327.

APPENDIX A

P/PWP VALUES FOR THE MEMBRANES

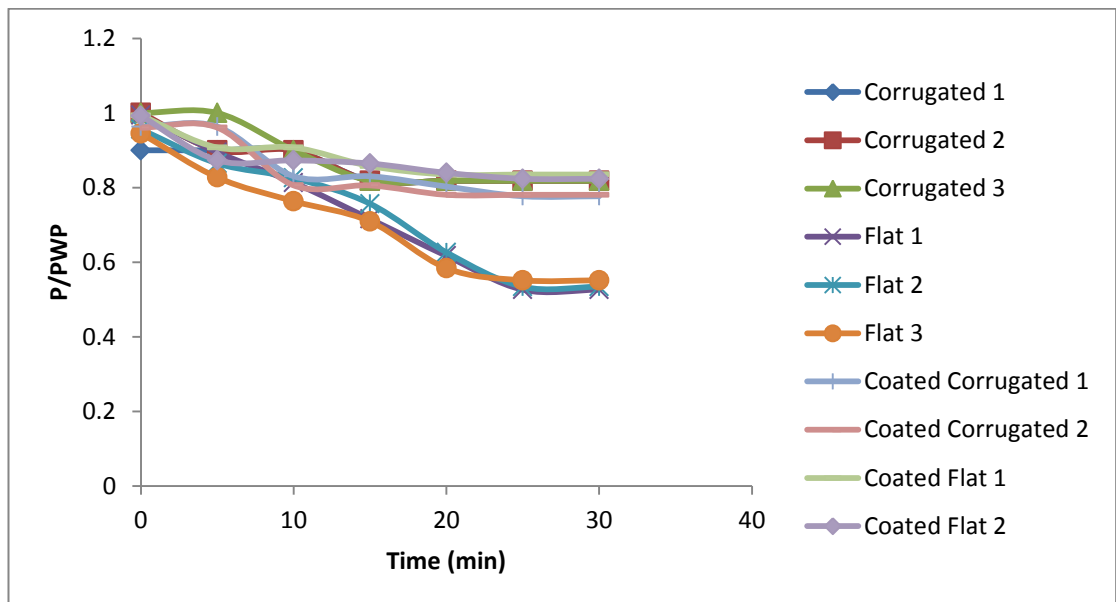


Figure A.1: Comparison of P/PWP Values for Coated and Uncoated Flat and Corrugated Membranes for Re=444

APPENDIX B

CALCULATION OF REYNOLDS NUMBERS AND PWP

$$\text{Cross Flow Velocity} = \frac{Q}{A}$$

Where Q represents the volumetric flow rate in m³/s and A represents the area perpendicular to the flow in m².

Reynolds Number was then calculated using the cross flow velocity:

$$Re = \frac{DV\rho}{\mu}$$

Where Re represents the Reynolds Number, D implies the hydraulic diameter of the flow in meters, V is the cross flow velocity in m/s, ρ is the feed stream density in kg/m³ and μ is the viscosity of the feed.

Hydraulic diameter, on the other hand, was calculated using the equation below:

$$Re = \frac{4A}{P}$$

Where A represents the perpendicular area to the flow in m² and P is the wetted perimeter in meters.

$$PWP = \frac{J}{TMP}$$

Where PWP is the pure water permeance in L/m²hbar, J is the flux in L/m²h on membrane area and TMP is the trans membrane pressure in bar.

After measuring the fluxes at 1, 0.75, 0.50 and 0.25 bar; flux vs pressure graph was plotted, slope of which gave the pure water permeance.

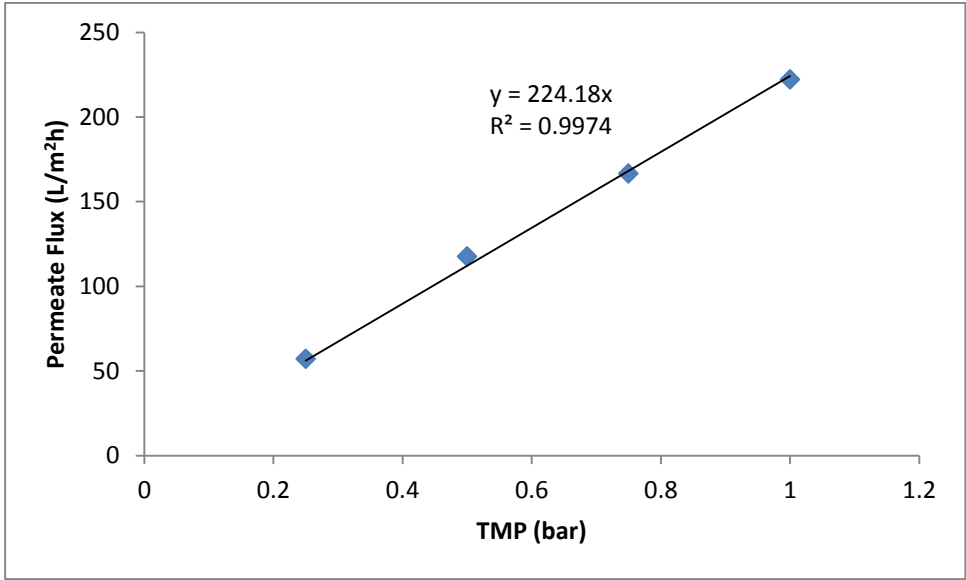


Figure B.1: TMP versus Permeate Flux of a Corrugated Membrane with a Pure Water Permeance Value of 224.18 L/m²hbar

APPENDIX C

BSA REJECTION CALCULATIONS

The percent BSA retentions of the membranes were calculated using the equation below:

$$\% \text{ Retention} = \left(1 - \frac{C_p}{\left(\frac{C_f + C_r}{2}\right)}\right) \times 100$$

Where C_f is the feed concentration, C_p is the permeate concentration and C_r is the retentate concentration.

Calculating also the permeance during filtration for each sample, a graph of permeance and percent retention versus permeate volume was plotted for each membrane.

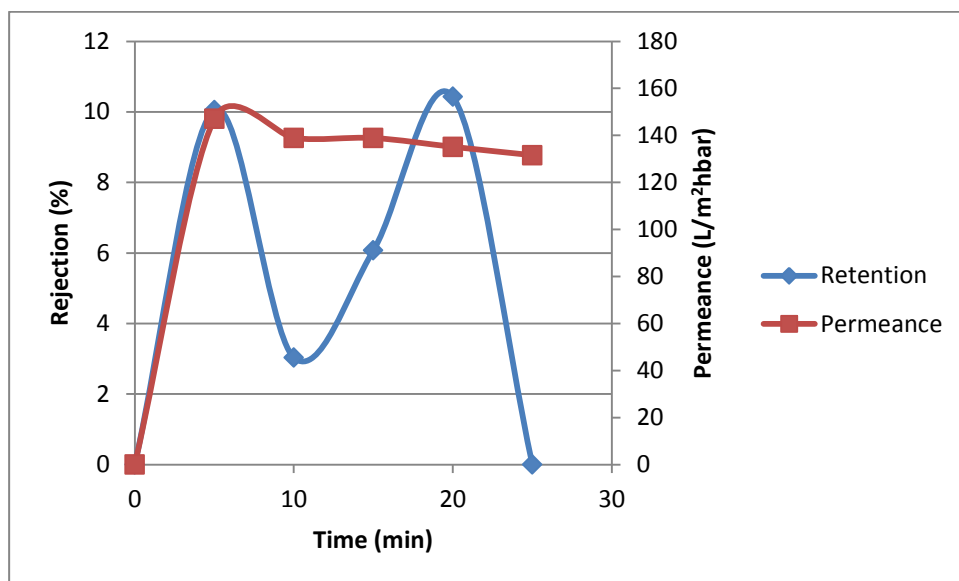


Figure C.1: Change of Retention and Permeance of a Polydopamine Coated Corrugated Membrane

APPENDIX D

FOULING RESISTANCE CALCULATIONS

$$J = \frac{TMP}{\mu \times R_{tot}}$$

Where J is the flux in L/m²h, TMP is the trans membrane pressure in bar, μ is the permeate viscosity and R_{tot} is the total flow resistance on the membrane in m⁻¹.

Using the total resistance, and the intrinsic resistance that was calculated during pure water permeance tests, fouling resistances of the membranes were calculated from the equation below:

$$R_f = R_{tot} - R_m$$

Where R_f is the fouling resistance, R_{tot} is the total resistance and R_m is the intrinsic membrane resistance to the flow in m⁻¹.

A sample calculation for a membrane with a PWP of 222.22 L/m²hbar and a permeance of 200 L/m²hbar during yeast filtration under 1 bar is:

$$R_{tot} = \frac{TMP}{\mu \times J}$$

$$R_{tot} = \frac{1 \text{ bar} \times \frac{10^5 \text{ Pa}}{1 \text{ bar}}}{0.89 \times 10^{-3} \text{ Pa} \cdot \text{s} \times 200 \frac{\text{L}}{\text{m}^2 \text{h}} \times \frac{1 \text{ h}}{3600 \text{ s}} \times \frac{1 \text{ m}^3}{1000 \text{ L}}}$$

$$R_{tot} = 2.02 \times 10^9 m^{-1}$$

$$R_m = \frac{1 \text{ bar} \times \frac{10^5 Pa}{1 \text{ bar}}}{0.89 \times 10^{-3} Pa \cdot s \times 222.22 \frac{L}{m^2 h} \times \frac{1 h}{3600 s} \times \frac{1 m^3}{1000 L}}$$

$$R_m = 1.82 \times 10^9 m^{-1}$$

$$R_f = R_{tot} - R_m$$

$$R_f = 2.02 \times 10^9 - 1.82 \times 10^9 = 2.02 \times 10^8 m^{-1}$$